

Chapter 1

Introduction

The progress of the CMOS technology in recent years has reached the point where CMOS processors can outperform bipolar processors. Development of DRAM technology focuses on minimization of the area occupied by the memory cell, while microprocessor performance is dominated by the length of the transistor gate and by the number of interconnect layers. According to the National Technology Roadmap for Semiconductors (NTRS) [1], DRAM half-pitch size, which is 250nm in 1997 technology, will reach 100nm by year 2006. As the feature size shrinks, the number of interconnections between gates increases and wirability becomes an important factor and needs to be addressed and analyzed carefully. On the other hand, the number of metal layers has to be reduced to a minimum to reduce the manufacturing costs. These two conflicting requirements ask for innovative wiring schemes such as dividing a logic block into several blocks. To increase the wire density, lower level metal line width needs to be scaled down approximately at the same rate as gate length. Consequently, the line resistance becomes large, causing not only additional RC delays but reliability problems like electromigration (EM). The use of new materials like copper, which has higher conductivity and higher resistance against EM than aluminum, and low dielectric constant materials like polyimides or xerogels, which will give lower capacitance overall than silicone dioxide, is inevitable in future on chip interconnect design. Additional improvement can be achieved by using high aspect ratio of the wire (thickness/width) since this can give higher wiring density without increasing the resistance. However, this kind of wire can increase unwanted coupling effects and cause false switching. Crosstalk can be deadly especially when dynamic logic families such as domino are used, and

wiring pitch, as well as the aspect ratio of the wire, should be determined properly to keep these effects within tolerable limits.

While most of the attention is focused on low level metals, the importance of the higher level metals, which carry signals over long distance, is unfairly de-emphasized since they are a small portion of total wiring. However, these global wires become longer as feature size shrinks and delays due to these wires can be an important portion of the clock cycle [2]. NTRS 97 [1] predicts that the wire delays will dominate device delays in future generations (deep submicron) due to the excessive resistance caused by the scaled line width. Even though this result is considered a pessimistic estimation due to some unreasonable assumptions made in this study, there is little doubt about the importance of the interconnect delays on total delay estimation in future generations [2]. This increasing wire delay has received a lot of attention, especially from the design community, because the ordinary design flow that has been used so far would not be applicable for the future generation. Typically, timing analysis has been achieved prior to the physical design based on simple device capacitance and wire capacitance models. Then extraction is done, followed by layout verification. However, as interconnect delay becomes an important part of the total delay, an accurate timing analysis is impossible without prior knowledge of the layout. One of the suggested solutions is using many blocks with limited number of gates [3]. Once the number of gates in each block is limited to a certain number, the average wire length becomes shorter in future generations, and interconnect delay no longer dominates device delay. However, this technique brings up another problem. As the number of gates used in a block decreases, there need to be more global wires that connect between hundreds and thousands of small blocks, so a major issue is shifted towards global wiring. Also, more metal layers are required due to the increasing number of the global wires. Whether one agrees with this solution technique, there is little dispute on the increasing importance of the global wires in timing analysis and physical design in future generations. In high

performance processors, the cross-sections of these global wires need to be big enough to carry signals without RC delays. To reduce the delay further, repeaters are inserted, yet careless design can actually increase the total delays since repeaters can increase loading capacitance for the previous stage. Increasing the driver size produces larger current and reduces the delay. However, this can increase the capacitance loading due to the larger device capacitance and also consumes more power. Increasing driver size means reduction of driver impedance, sometimes to the point where it is smaller than the characteristic impedance of the line. The inductance and resistance variation from low frequency to high frequency can be an important factor in determining accurate total delay in this situation [4]. As the chip speed exceeds giga-hertz range, these frequency dependent effects become more important. Transmission line effects become even more important for multichip modules and printed circuit boards. Efficient characterization of frequency dependencies in these structures is quite a challenging task. In micro strip line type of structures, not only skin effect but current crowding effect due to the wide ground plane can change the inductance value dramatically.

In this dissertation, a new series impedance extraction technique particularly for higher level on-chip interconnects as well as off-chip interconnects (i.e., PCB, MCM) will be introduced. The conventional way of extracting frequency dependent series impedance is through the Volume Filament Method (VFM) [5, 6] where a conductor is divided into many filaments where constant current is flowing along the each filament. In recent years, numerical acceleration techniques [7] have been applied to VFM to speed the large matrix inversion procedure, and different segmentation techniques [8] have been used to apply VFM to various cross-sections other than rectangular shapes. However, in VFM, the dimensions of the filaments have to be smaller than a skin depth at a given frequency, which can require a lot of filaments, large memory, and considerable CPU time regardless of the improvement in the numerical techniques.

A generally more attractive approach is a "surface integral equation method" [8, 9] where only surface currents are modeled, requiring much less memory usage and CPU time for simulation. This approach, however, requires calculation of surface current distributions using the method of moments that can be numerically expensive, especially when there are sharp corners. This technique may also have numerical problems at low frequency when current distribution is almost uniform across the cross-section of the conductors, as opposed to the high frequency limit when the current density is well approximated as a surface current.

Recently, a new surface impedance boundary condition, the Effective Internal Impedance (EII), has been developed [10-12]. This new boundary condition can be easier to approximate because of its localized characteristics. That is, this boundary condition is relatively independent of the presence of the other conductors and can be approximated from low frequency to high frequency the using surface impedance of an isolated conductor. Because of these characteristics, this boundary condition can be used in conjunction with external solvers to characterize multi-conductor transmission lines without solving complicated boundary conditions through the method of moments.

Simulation methods for coupled transmission lines in the time domain have gotten a lot of attention in recent years due to the ever-increasing device speed and densely packed interconnects. The time domain simulation methods are largely categorized into three techniques: full-wave technique, transfer function analysis, and RLC equivalent circuit analysis. The full-wave techniques based on solving Maxwell's equations include finite difference time domain method (FDTD) [13] and partial element equivalent circuits (PEEC) [5, 14, 15]. These approaches are useful to obtain accurate time domain waveforms for complex three-dimensional structures, but can be computationally expensive.

The other methods that utilize an approximation of the transfer function of the transmission line system can be very efficient when the frequency dependent

characteristics of the systems are known. In these kinds of techniques, to accurately simulate transient responses of the lossy transmission lines, all the frequency dependent resistance and inductance have to be included in the model. This usually requires diagonalization of propagation function or transfer function using eigenvectors and eigenvalues that are frequency dependent. Unfortunately, there are stability issues associated with poles on the right hand side of the complex plane that one has to cope with when the eigenvector matrix is represented with polynomial rational functions. Also, the application of this approach to the simulation of circuits including nonlinear drivers can be difficult. However, the attraction of this method is only the input port and the output port of the transmission lines have to be characterized, so avoiding a large number of nodes.

The techniques based on the equivalent circuit that model frequency dependent characteristics of the transmission lines with frequency independent RLC circuit [16-18] are less appealing, mainly because the number of the nodes involved becomes large especially when the rise time of the input becomes short. However, one of the advantages of this equivalent RLC circuit modeling is that one can avoid the calculation of the frequency dependent series impedance of the lines. That is, most other techniques based on transfer functions require frequency dependent samples, e.g., series impedance, at several frequency points through either simulation or measurement to approximate transfer function, while values of the circuit elements used in RL circuit model can be determined directly from the geometry of the conductor. Also, RLC models can be directly simulated with existing circuit simulators like SPICE with other nonlinear devices. In this dissertation, a frequency independent RLC equivalent circuit model is presented. This equivalent circuit can accurately model the frequency dependencies of the multi-conductor transmission lines with a relatively small number of circuit elements. Then, to reduce the number of nodes, the method of characteristics and the finite difference method are applied

to the lossless-like equation that results from solving the telegrapher's equation with a recursive formulation.

In chapter 2, the surface ribbon method is reviewed. This method is first introduced in [11] and successfully applied to the general 3-dimensional problems [10]. In this chapter, thorough numerical and theoretical approaches behind the SRM will be introduced to explain why and how this technique works. In chapter 3, SPICE equivalent circuit model that captures frequency dependent effects is introduced. Simple rules to construct this model are introduced and application of this model to multi-conductor transmission lines is explored. In chapter 4, new time domain multi-conductor transmission line equations are derived based on SRM and the SPICE equivalent model. These new equations are used in the method of characteristics and the finite difference methods to obtain time domain waveforms including frequency dependent effects.

Chapter 2

Series Impedance Calculation Using Surface Ribbon Method (SRM)

In high performance integrated circuit, an accurate estimation of the delays or coupled noise due to the finite conductivity and the presence of other conductors becomes more difficult. The ever-increasing speed of the digital circuits demands broad bandwidth characterization of the frequency dependent transmission lines to get accurate transient waveforms. The advances in time domain simulation techniques of lossy transmission lines in recent years are quite remarkable, yet almost every technique requires some frequency domain samples of series impedance of the transmission lines, which is becoming much more complicated task as the integrated circuit technology advances. The conventional, yet numerically expensive way of extracting frequency dependent series impedance, is through Volume Filament Method (VFM) [5, 6]. To overcome the inefficiency of the VFM, techniques based on surface currents [8, 9] have been introduced. However, it is not always easy to satisfy the boundary conditions, and these techniques are limited to the high frequency range where the skin depth is much smaller than the thickness of the conductor. A new impedance boundary condition, the Effective Internal Impedance (EII), is much more useful for series impedance calculations due to its localized characteristics. This new boundary condition is easier to predict due to its localized behavior throughout the frequency band of interested.

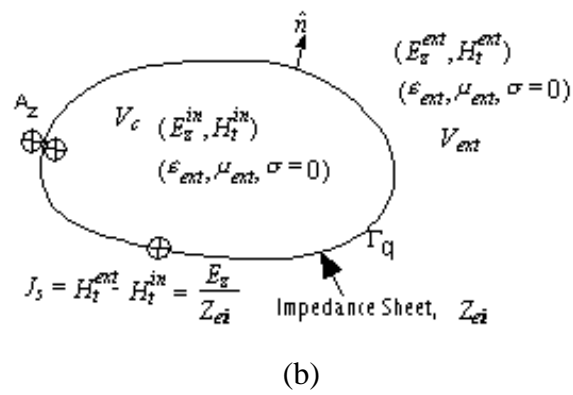
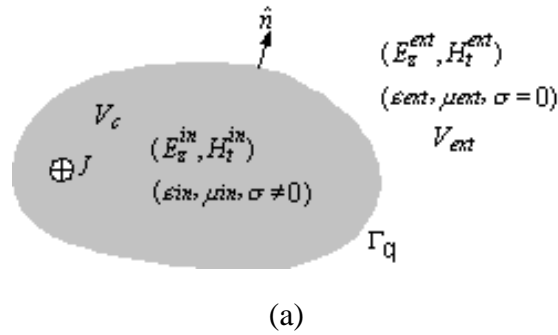


Figure 2.1: Series impedance calculation of lossy conductor using surface equivalent theorem. (a) Original problem where volume current is flowing through a conductor. (b) Equivalent problem where conducting body is replaced with external medium and volume current replaced with equivalent surface current. Continuity of vector magnetic potential is assumed.

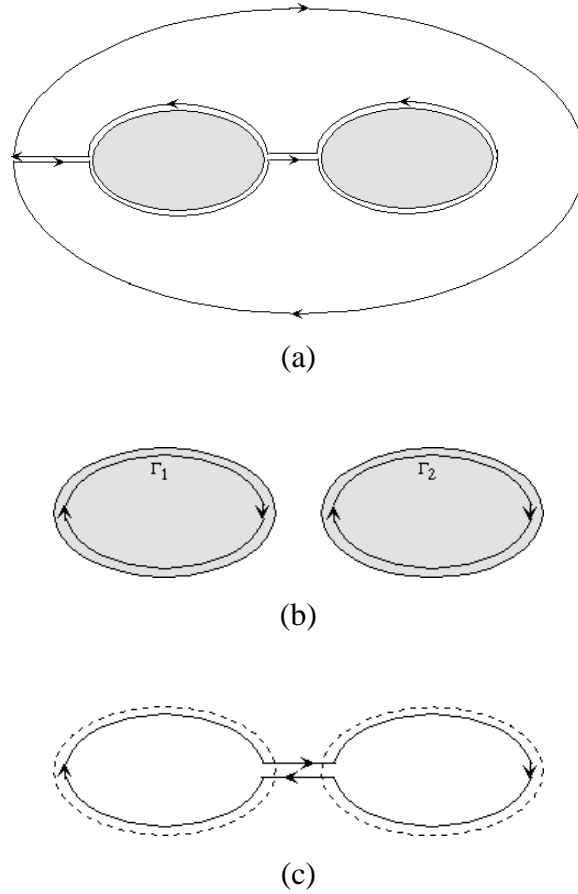


Figure 2.2. Integral path along the perimeter of two conductors. (a) Integral path for the external region of the conductors. (b) Integral path for the internal region of the conductors (before applying the surface equivalence theorem). (c) Integral path for the internal region of the conductors (homogeneous medium).

2.1 Effective Internal Impedance (EII)

The EII was first introduced in [19] and several approximation methods for the EII were introduced in [10]. However, an accurate theoretical concept of this quantity has not been available. This EII is an essential quantity in the surface ribbon method (SRM) and needs to be identified accurately to justify the SRM. The numerical derivation for the SRM introduced in [10] gives a somewhat incomplete

for the EII. In this section, thorough theoretical concept of the EII is introduced using the surface equivalent theorem.

According to the equivalence theorem, the original problem can be replaced with equivalent surface currents as long as this current generates the correct fields outside of the conductors, while the fields inside of the conductor can be assumed to be arbitrary. This allows one to replace the medium inside the conductor boundaries with the same medium as the external region. Consequently, an external Green's function can be used everywhere in the integral equations.

In formulating a surface boundary condition the fields inside of the conductors are usually assumed to be zero [20], but here we assume the vector magnetic potential is continuous across conductor surfaces, and the equivalent surface current is defined as the difference between original tangential magnetic field and internal tangential magnetic field generated in this new equivalent problem. Figure 2.1 shows the original problem and the equivalent problem explained here. The original problem is replaced with an equivalent problem with equivalent surface current defined as a ratio of the longitudinal electric field and the difference of the two tangential magnetic fields on the surface. Of course, it might seem that this new approach would make the problem much more complicated, but as will be demonstrated later, the surface impedance boundary condition satisfying this new problem, the effective internal impedance (EII), is much more localized than the SIBC from low to high frequencies. The surface integral equation before applying the equivalence theorem for the exterior region can be obtained from [8]

$$\oint dr' G_{ext}^1(r, r') \mu H_t(r') + \oint dr' [G_{ext}^2(r, r') - p(r') \delta(r - r')] A_z(r') = 0 \quad , \quad (2.1)$$

where H_t and A_z are the tangential magnetic field and longitudinal magnetic vector potential respectively, $p(r')$ is the position dependent coefficient describing source strength distribution (often assumed without justification to be 0.5 [8, 10]), and G_{ext}^1 and G_{ext}^2 are the free space external Green's function and its derivative with respect

to the surface normal, respectively, and the integral is carried out along the perimeter of all conductors (see Figure 2.2 (a)). For the interior region,

$$\oint_{\Gamma_q} dr' G_q^1(r, r') j\omega\mu H_t(r') - \oint_{\Gamma_q} dr' [G_q^2(r, r') + [1 - p(r')] \delta(r - r')] E_z(r') = 0 \quad , \quad (2.2)$$

where G_q^1 and G_q^2 are the Green's function and its normal derivative for conductor q , respectively, and the integral is carried out along the each individual conductor perimeter Γ_q (see Figure 2.2 (b)). Equation (2.1) and (2.2) have to be solved

together with the requirement that

$$\oint_{\Gamma_q} dr' H_t = I_q \quad , \quad (2.3)$$

where I_q is the total current carried by conductor q .

After applying the equivalence theorem, the Green's function that appears in equation (2.2) can be replaced by the free space Green's function used in (2.1). In this paper we use continuity of the vector magnetic potential across conductor surfaces to complete the definition of the EII. Equation (2.1) for the exterior region becomes

$$\oint dr' G_{ext}^1(r, r') \mu H_t^{ext}(r') + \oint dr' [G_{ext}^2(r, r') - p(r') \delta(r - r')] A_z(r') = 0 \quad , \quad (2.4)$$

where H_t^{ext} is the external tangential magnetic field. The interior region equation (2.2) becomes

$$\oint dr' G_{ext}^1(r, r') \mu H_t^{in}(r') + \oint dr' [G_{ext}^2(r, r') + [1 - p(r')] \delta(r - r')] A_z(r') = 0 \quad , \quad (2.5)$$

where H_t^{in} is the internal tangential magnetic field and since the medium is uniform in our new equivalent problem, the integral is now carried out along the entire surface of inside of the conductor instead of the surface of the conductor q (see Figure 2.2 (c)). If the values of external tangential magnetic field and magnetic vector potential are exactly known in equation (2.4) (here, magnetic vector potential

is related to magnetic field by $\vec{A} = \nabla \times \mu \vec{H}$), the position dependent coefficient $p(r')$ can be determined, and then H_t^{in} can be found from equation (2.5).

For this new equivalent problem, the relationship between the longitudinal electric field and the difference of the tangential magnetic fields across the equivalent surface impedance sheet is called the effective internal impedance (the EII, to distinguish it from the SIBC), and is then

$$Z_{eii}(\omega, r') = \frac{E_z(r')}{H_t^{ext}(r') - H_t^{in}(r')} = \frac{E_z(r')}{J_s(r')} , \quad (2.6)$$

where Z_{eii} is the EII and J_s is the equivalent surface current density.

To compute the integrated quantities of series impedance using the EII approach, power applied, power dissipated, and magnetic energy stored in the equivalent problem are found using

$$-\int_S ds \nabla \Phi^q \cdot \vec{J}_s^* = \int_S ds Z_{eii} |J_s|^2 + j\omega \int_S ds \vec{A} \cdot \vec{J}_s^* , \quad (2.7)$$

where S is the conductor surface and Φ is the electric potential. The left-hand side of the equation (2.7) is the power applied, the first term of right-hand side is the power dissipated, and the second term corresponds to the magnetic energy stored.

From the power dissipation term in (2.7), resistance can be calculated using

$$R_q^{srm}(\omega) = \frac{\oint_{\Gamma_q} dr' \operatorname{Re} \{ Z_{eii} |J_s|^2 \}}{\left| \oint_{\Gamma_q} dr' J_s \right|^2} \cdot l_q , \quad (2.8)$$

where l_q is the length of the line q . Internal inductance of conductor q and total external inductance are calculated from the stored magnetic energy term,

$$\begin{aligned}
L_{in,q}^{srm}(\omega) &= \frac{\mu \int_{V_q} dv \vec{H}^{in} \cdot \vec{H}^{in*}}{|I_q|^2} = - \frac{\int_{S_q} ds \hat{n} \cdot \left(\vec{A} \times \vec{H}^{in*} \right)}{\left| \oint_{\Gamma_q} dr' J_s \right|^2} \\
&= - \frac{\oint_{\Gamma_q} dr' \text{Im} \left\{ E_z H_t^{in*} \right\}}{\omega \left| \oint_{\Gamma_q} dr' J_s \right|^2} \cdot I_q
\end{aligned} \tag{2.9}$$

and

$$\begin{aligned}
L_{ext}^{srm}(\omega) &= \frac{\mu \int_{V_{ext}} dv \vec{H}^{ext} \cdot \vec{H}^{ext*}}{\sum_{q=1}^m |I_q|^2} = \frac{\int_S ds \hat{n} \cdot \left(\vec{A} \times \vec{H}^{ext*} \right)}{\sum_{q=1}^m \left| \oint_{\Gamma_q} dr' J_s \right|^2} \\
&= \sum_{q=1}^m \left(\frac{\oint_{\Gamma_q} dr' \text{Im} \left\{ \left(E_z + \nabla \Phi^q \right) H_t^{ext*} \right\}}{\omega \left| \oint_{\Gamma_q} dr' J_s \right|^2} \right) \cdot I_q \quad ,
\end{aligned} \tag{2.10}$$

where V_{ext} is the volume exterior to the conductors. The surface inductance due to the magnetic energy stored by the impedance sheet is given by

$$L_{sur,q}^{srm}(\omega) = \frac{\int_S ds \text{Im} \left\{ Z_{eii}^q |J_s|^2 \right\}}{\omega |I_q|^2} = \frac{\oint_{\Gamma_q} dr' \text{Im} \left\{ Z_{eii}^q |J_s|^2 \right\}}{\omega \left| \oint_{\Gamma_q} dr' J_s \right|^2} \cdot I_q \quad . \tag{2.11}$$

Finally, the sum of internal, external, and surface inductances from (2.9), (2.10), and (2.11) gives the total series inductance for the transmission line in the EII formulation.

To validate equations (2.8) to (2.11), a similar procedure can be used to derive the equations for series impedance using the boundary element method [8, 10]. Using the exact exterior magnetic and electric fields from the original problem,

it can be shown that the resistances given by (2.8) are identical to the original problem, that the external inductance given by (2.10) is identical to the original problem, and the sum of (2.9) and (2.11) is identical to the internal inductances in the original problem.

The obvious difference between this new approach and the boundary element method (BEM) using SIBC is rather than excluding the conductor interior from the problem by assuming zero interior field, continuation of vector magnetic potential has been assumed. Consequently, the interior fields are taken care of through this new impedance boundary condition. The similarity between the BEM and the SRM is that only the quantities on the surface of the conductor are characterized to achieve numerical efficiency.

2.2 Surface Ribbon Method

The series impedance calculations based on energy conservation that was introduced in the previous section is a time-consuming task. A much simplified formulation can be derived directly from (2.4), (2.5), and (2.6). By subtracting (2.5) from (2.4) and applying (2.6) the following integral equation results for an m conductor system

$$\sum_{q=1}^m \oint_{\Gamma_q} dr' \{ j\omega\mu G_{ext}^1 + \delta(r-r')Z_{eii}(r') \} J_s(r') + \sum_{q=1}^m \oint_{\Gamma_q} dr' \delta(r-r') \nabla_z \Phi^q = 0 \quad . \quad (2.12)$$

Each conductor perimeter Γ_q can be further divided into N_q segments, each with sub section $C_{q,k}$, where these pieces represent current-carrying “ribbons” of width

$w_{q,k} = \int_{C_{q,k}} dr$. Equation (2.12) then becomes

$$Z_{eii}^{q,k}(r)J_s^{q,k}(r) + j\omega\mu \sum_{i=1}^m \sum_{j=1}^{N_i} \int_{C_{i,j}} dr' J_s^{i,j}(r') G_{ext}^1(r, r') = -\nabla_z \Phi^{q,k}, \quad (2.13)$$

where $Z_{eii}^{q,k}$ and $J_s^{q,k}$ are respectively, the effective internal impedance and sheet current density on the k^{th} ribbon ($k = 1, 2, \dots, N_q$) of the q^{th} conductor ($q = 1, 2, \dots, m$) at a given frequency, and the second term on the left hand side represents contributions from self and mutual inductances. For a two dimensional case $G_{ext}^1(r, r') = -\frac{1}{2\pi} \ln|r - r'|$. If the ribbons are narrow enough that the sheet current density is constant across each ribbon, integrating over the k^{th} ribbon yields

$$\frac{I_s^k}{w_k} \int_{C_k} dr Z_{eii}^k(r) + j\omega\mu \sum_{i=1}^N \frac{I_s^i}{w_i} \int_{C_k} \int_{C_i} dr' dr G_{ext}^1(r, r') = -\int_{C_k} dr \nabla_z \Phi^k, \quad (2.14)$$

where I_s^k is the total sheet current carried by the k^{th} ribbon, and for simplicity the double superscript (q, k) has been replaced with the single superscript k ($k = 1, 2, \dots, N$, $N = N_q \times m$). Finally,

$$\overline{Z_{eii}^k} I_s^k \frac{l_k}{w_k} + j\omega\mu \sum_{i=1}^N \frac{I_s^i l_k}{w_k w_i} \int_{C_k} \int_{C_i} dr' dr G_{ext}^1(r, r') = \Phi_1^k - \Phi_2^k, \quad (2.15)$$

where $\Phi_1^k - \Phi_2^k$ is voltage drop along the ribbon k , $\overline{Z_{eii}^k}$ is the EII averaged over the width of ribbon k , and l_k is the length of ribbon k , which is assumed to be 1 in a two dimensional problem. Equation (2.15) can be expressed as an $N \times N$ matrix equation

$$[(Z_{eii}] + j\omega[L])[I] = [V], \quad (2.16)$$

where $[Z_{eii}]$ is an $N \times N$ diagonal matrix made up of the $\overline{Z_{eii}^k}/w_k$ and $[L]$ is a matrix consisting of self and mutual inductances between surface ribbons. This approach is called the surface ribbon method (SRM). If $[Z_{eii}]$ is known (2.16) can be used to

calculate resistance and inductance directly, as is done in the volume filament method [5, 6]. As shown in the following section, the EII has relatively localized characteristics, allowing $[Z_{eii}]$ to be easily approximated. The similarity between the SRM and the VFM is that all the series impedance parameters (left hand side of 2.16) are either known (VFM) or can be approximated with analytical form (SRM). Therefore, most of the computation time is dedicated to the inversion of the series impedance matrix. For this reason, the efficiency of the SRM over the VFM or the BEM is tremendous.

2.3 Characteristics of the EII

To calculate the exact EII, the volume filament technique can be used to find the external magnetic and electric fields and the vector magnetic potential, then these values are used in (2.4) and (2.5) to calculate the internal magnetic field, and finally the EII's can be found using (2.6). Figure 2.3 shows a comparison between the EII values for two circular conductors with radii 1 mm separated by 0.2 mm, 20 mm, and 200 mm, and the surface impedance of an isolated circular conductor given by [21],

$$Z_{cir} = \frac{j\sqrt{j\omega\mu\sigma}}{\sigma} \frac{J_0\left(ja\sqrt{j\omega\mu\sigma}\right)}{J_1\left(ja\sqrt{j\omega\mu\sigma}\right)}, \quad (2.17)$$

where a is the radius of the conductor. The most interesting characteristics of the EII is the position independence of the real part at low frequency, as shown in figure 2.3(a). All real parts of the EII are almost constant and are quite close to the surface impedance of the isolated conductor calculated from (2.17). The imaginary parts do have a position dependence, especially when two conductors are very close to each

other. However, this dependence diminishes quickly as the two conductors are separated, with values of $\text{Im}(\text{EII})$ being approximately the average of that obtained from (2.17). At high frequency, the internal fields of the conductors approach zero, and the EII calculated from (2.6) is expected to approach to the SIBC which is accurately approximated by (2.17) in the high frequency limit. Figure 2.3(b) shows that this does indeed occur. In other words, (2.17) can be used as an approximation of the EII to calculate series impedance of circular conductors regardless of the frequency or proximity of other conductors (i.e. $\overline{Z_{eii}^k} \approx Z_{cir}$ in (2.15) and (2.16)). To support this point, the series impedance of two circular conductors separated by 0.2 mm is calculated and compared with the volume filament method as shown in figure 2.4. Here, a polygon with degree N shown in figure 2.4(a) is used instead of a circular conductor to simplify the calculation of the mutual inductance between ribbons. Figure 2.4(b) indicates (2.17) is indeed a good approximation of the EII for series impedance calculation even when conductors are very close to each other.

The EII values for square conductors with width 25 μm and separated by 5 μm and 50 μm have also been calculated. It is impossible to calculate exactly the SIBC of isolated square or rectangular conductors due to the singularity at the corner, however, it can be approximated [22-26]. Detailed EII characteristics of a square conductor will be discussed in next section (Figure 2.7 and 2.8). At high frequency, the surface impedance of an infinitely wide and thick conductor given by

$$Z_s = \sqrt{\frac{\pi f \mu}{\sigma}} (1 + j) \quad (2.18)$$

is a reasonable approximation for the SIBC far from corners. Examination of other geometrical cases has confirmed that the EII is well approximated by the surface impedance of an isolated conductor, regardless of the presence of other conductors.

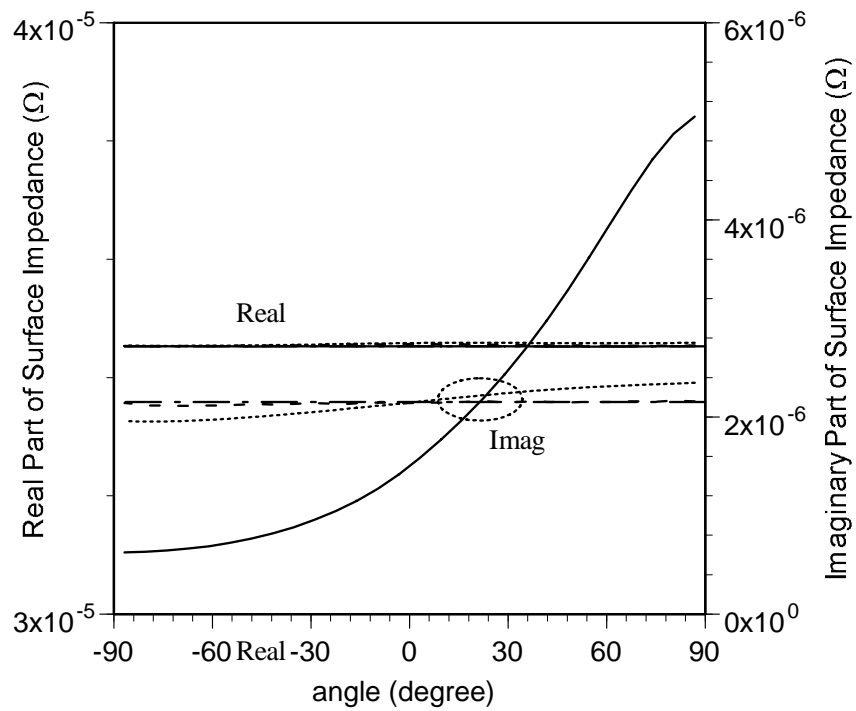
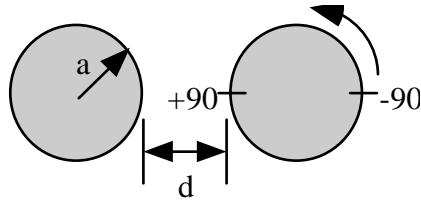


Figure 2.3(a): EII values for two circular conductor at $f=1\text{kHz}$. Solid line: $d=0.2\text{mm}$, dotted line: $d=20\text{mm}$, dashed line: $d=200\text{mm}$, dash-dotted line: equation (2.17).

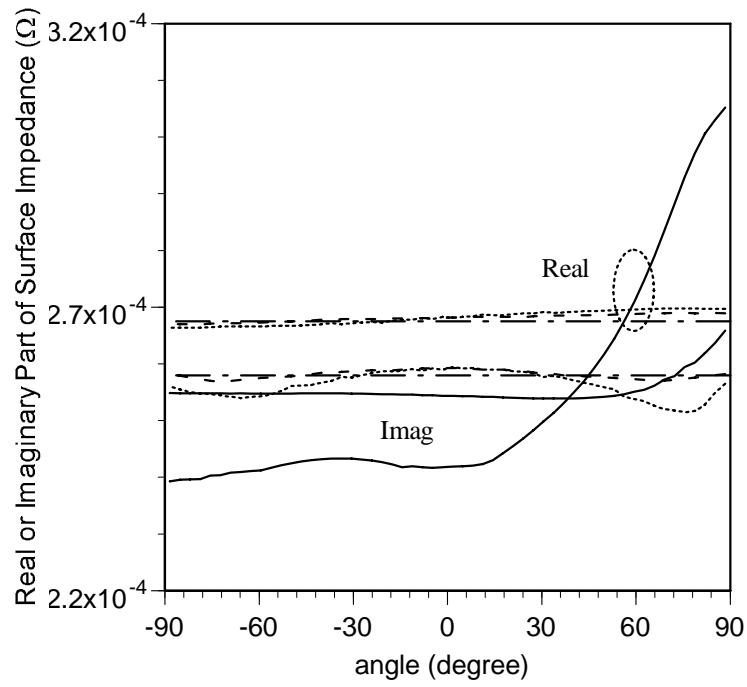
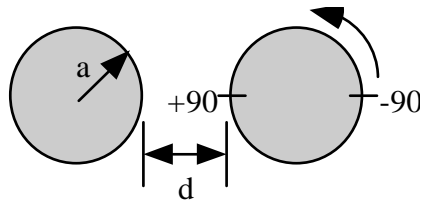


Figure 2.3(b): EII values for two circular conductor at $f=1\text{MHz}$. Solid line: $d=0.2\text{mm}$, dotted line: $d=20\text{mm}$, dashed line: $d=200\text{mm}$, dash-dotted line: equation (2.17).

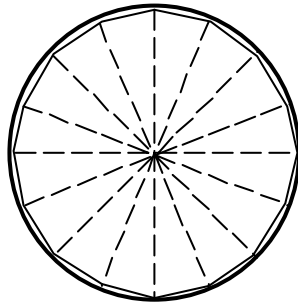


Figure 2.4(a): Segmentation for the estimation of the EII for a circular conductor.

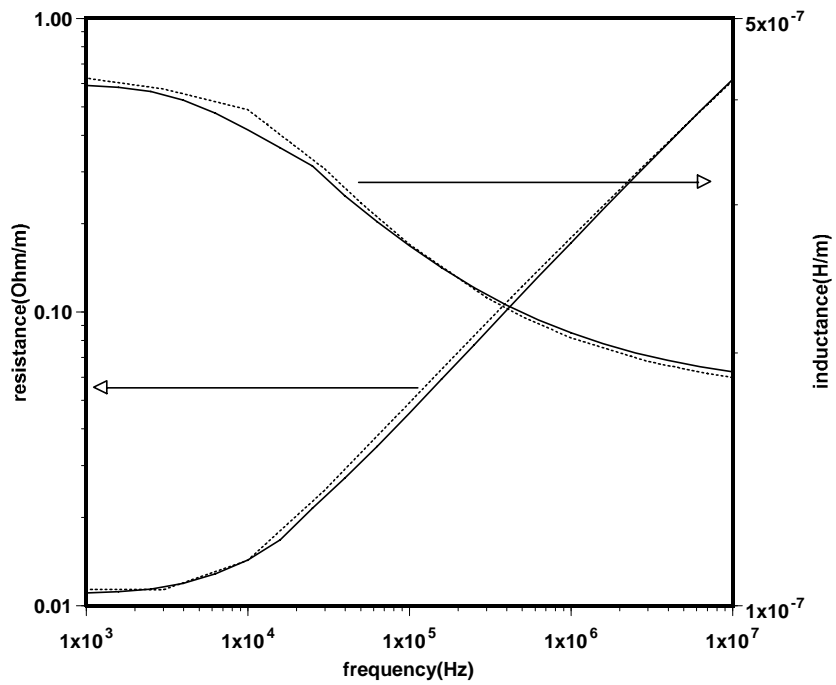


Figure 2.4(b): Series impedance of two circular conductors. radius=1mm, d=0.2mm.

2.4 Approximations of the EII

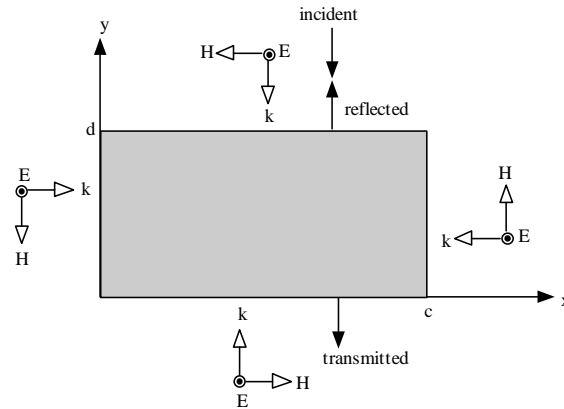


Figure 2.5): Plane wave model for the approximation of the EII of a rectangular conductor.

As it is indicated in previous section, rather than estimating the EII by solving complex integral equations with known electric and magnetic fields, the surface impedance of an isolated conductor can be used as an approximation of the EII. This is possible because the EII has fairly localized characteristics throughout a broad bandwidth, meaning the characteristics of the EII are hardly altered by the presence of other conductors [12]. Deely [23] introduced a modified surface impedance near the corner assuming transverse magnetic plane wave is normally incident onto all surfaces of the conductor, and Jingguo *et. al* [25, 26] extended this model to corners of arbitrary angle, transverse electric problems, and three dimensional structures.

Here, two different techniques for the approximation of surface impedance of an isolated conductor are introduced. Then the estimation from each technique will be compared with the EII that has been obtained through solving integral equations to see which approximation technique matches the EII better.

The first approximation technique is a plane wave model (PWM) [10]. In this model, surface impedance is found by assuming uniform TM plane waves

incident on four surfaces and reflected from interfaces (Figure 2.6a). The field quantities under these assumptions are repeated in this dissertation due to some misprint in [10]. They are

$$\vec{H}(x, y) = H_0 \left\{ \begin{array}{l} \hat{x} \left[\frac{e^{-\gamma y} - e^{\gamma(y-2d)} - \Gamma(e^{\gamma(y-2d)} - e^{-\gamma(y+d)})}{1 - \Gamma e^{-2\gamma d}} \right] \\ + \hat{y} \left[\frac{-e^{-\gamma x} + e^{\gamma(x-c)} + \Gamma(e^{\gamma(x-2c)} - e^{-\gamma(x+c)})}{1 - \Gamma e^{-2\gamma c}} \right] \end{array} \right\} \quad (2.19)$$

$$\vec{E}(x, y) = \hat{z} H_0 \sqrt{\frac{j\omega\mu}{\sigma}} \left\{ \begin{array}{l} \frac{e^{-\gamma y} + e^{\gamma(y-d)} + \Gamma(e^{\gamma(y-2d)} + e^{-\gamma(y+d)})}{1 - \Gamma e^{-2\gamma d}} \\ + \frac{e^{-\gamma x} + e^{\gamma(x-c)} + \Gamma(e^{\gamma(x-2c)} + e^{-\gamma(x+c)})}{1 - \Gamma e^{-2\gamma c}} \end{array} \right\}, \quad (2.20)$$

where $\Gamma = \frac{\eta_0 - \eta_m}{\eta_0 + \eta_m}$, and $\eta_0 = \sqrt{\frac{\mu_0}{\epsilon_0}}$, $\eta_m = \sqrt{\frac{j\omega\mu}{\sigma}}$. Γ is the reflection coefficient at

the interface between air and conductor. The impedance at the surface of the conductor can be obtained using

$$Z_s(\omega, x, y) = \frac{E_z(x, y)}{H_t(x, y)}, \quad (2.21)$$

where $H_t(x, y)$ is $H_x(x, y)$ on the top or bottom of the surface, $y = 0, d$, while $H_y(x, y)$ should be replaced in (2.21) on the side surfaces of the conductor, $x = 0, c$.

A second approximation technique is called a transmission line model (TLM). First, for a rectangular conductor, the conductor is segmented into four square corners and two flat rectangular sections, which are further divided into several rectangles and triangles as illustrated in figure 2.6b. Then the surface impedance of each section is the averaged surface impedance of the original rectangle at given location. To calculate surface impedance of each triangle and rectangle, transverse resonance [27] is applied. In transverse resonance method, a conductor cross-section is considered as non-uniform transmission line terminated

with open circuit at the load, and the input impedance is calculated and considered as the surface impedance. The surface impedance of central rectangular region in figure 2.6 is thus approximated using

$$Z_s = \sqrt{\frac{j\omega\mu}{\sigma}} / \tanh\left(\sqrt{j\omega\mu\sigma} \frac{t}{2}\right). \quad (2.22)$$

The surface impedance of the corner triangular section can be approximated using the input impedance of an isosceles triangle [19] as illustrated in figure 2.6,

$$Z_s = \frac{jW}{W_{iso}} \sqrt{\frac{j\omega\mu}{\sigma}} \frac{J_0(j\sqrt{j\omega\mu\sigma}h)}{J_1(j\sqrt{j\omega\mu\sigma}h)}, \quad (2.23)$$

where J_0 and J_1 are Bessel functions of the first kind.

In figure 2.7, the two surface impedance approximation techniques introduced here are compared with the EII at both low frequency and high frequency. Notice that the EII does not change much when the distance between two conductors varies from $5\mu\text{m}$ to $100\mu\text{m}$. At low frequency, both the TLM and the PWM averages the real part of the EII and approximates imaginary part of the EII very well. At high frequency, the PWM approximates the EII quite well, while the TLM effectively averages the EII. The biggest difference occurs at the corner of the conductor where fields are singular. Here, it has to be pointed out that these approximation techniques are for series impedance calculation of transmission lines, not for the calculation of field quantities. For this reason, the accurate approximation of the EII at the corners is not necessary and averaged approximation techniques like the TLM can be useful. This is because the parallel sum of the EII is the main factor in determining series impedance. Even though the PWM gives better approximation of the EII, the TLM has an advantage due to its flexibility to other geometrical shapes. The segmentation scheme for the TLM is much like finite element method discretization, and can be applied to obtain surface impedance of conductors with various cross-sections. Also, when a small number of discretizations is desired to reduce CPU time, the TLM gives better results than the PWM.

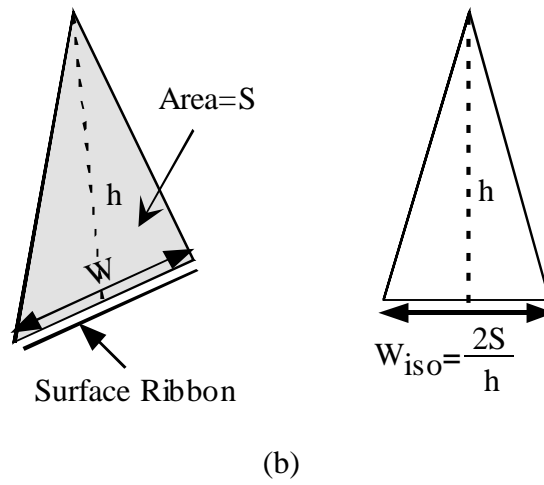
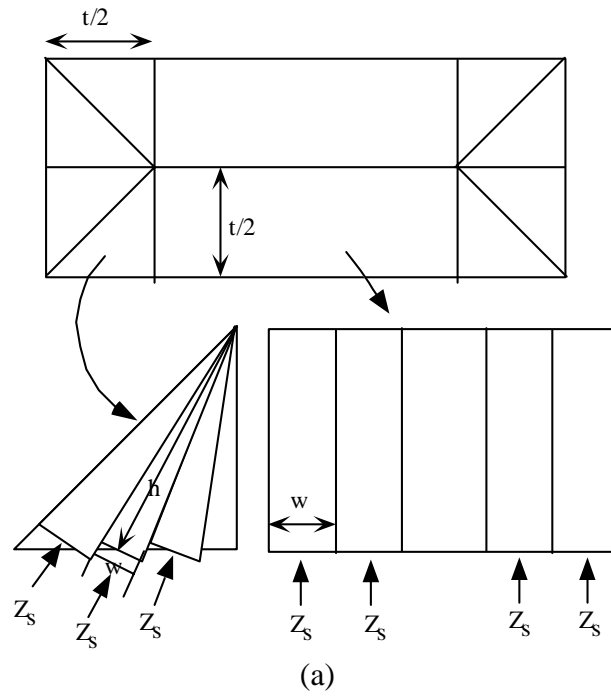


Figure 2.6: Segmentation of a rectangular conductor for the approximation of the EII using the transmission line model. (a) rectangular segmentation for the middle part of the conductor, triangular segmentation for the corner of the conductor. (b) EII approximation for an arbitrary triangle. Input impedance of an equivalent isosceles triangle is calculated using the transverse resonance method.

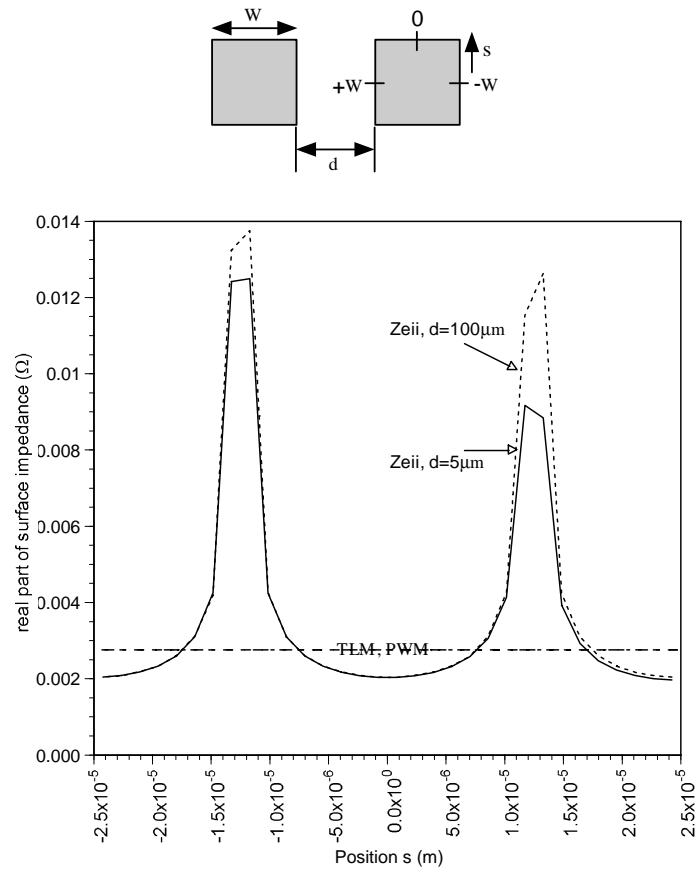


Figure 2.7(a): Real part of the EII values and their approximations at $f=1\text{kHz}$.

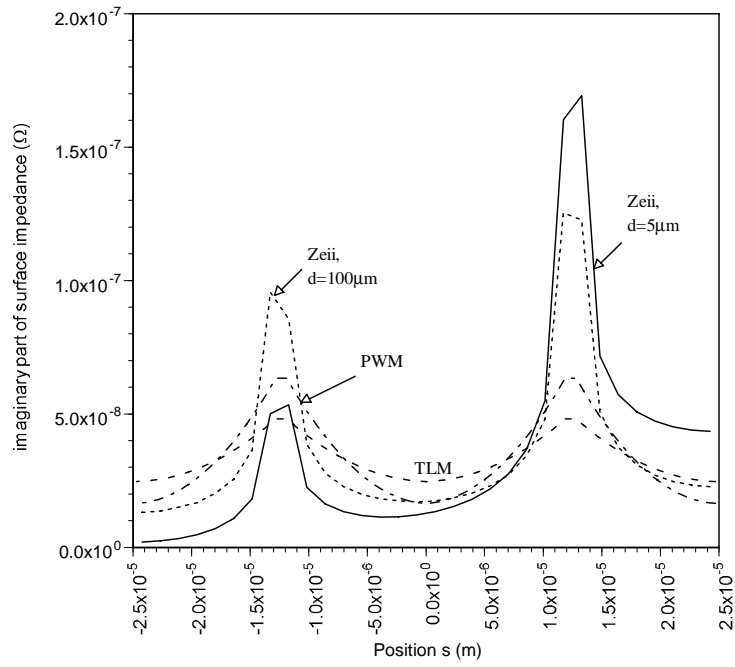


Figure 2.7(b) Imaginary part of the EII values and their approximations at $f=1\text{kHz}$.

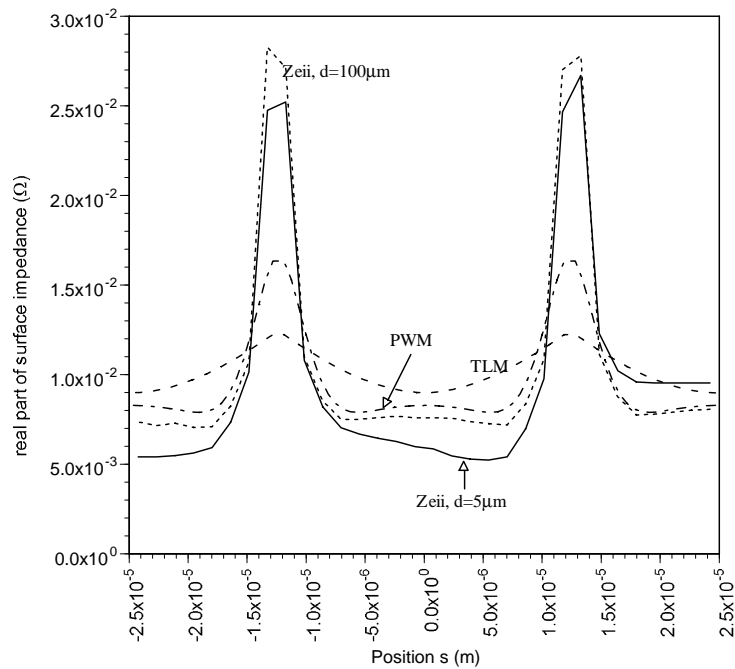


Figure 2.8 (a): Real part of the EII values and their approximations at $f=1\text{GHz}$.

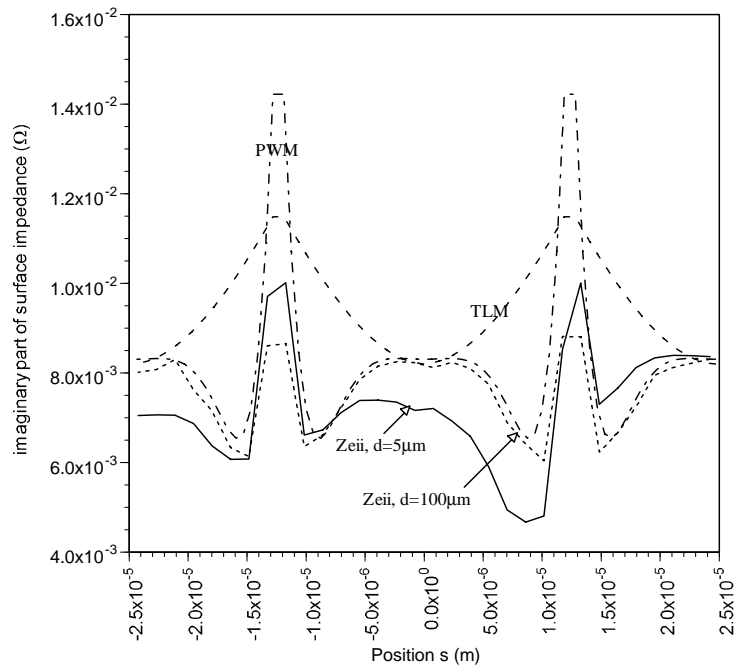


Figure 2.8(b): Imaginary part of the EII values and their approximations at $f=1$ GHz.

2.5 Applications of the SRM

2.5.1 Rectangular Conductor

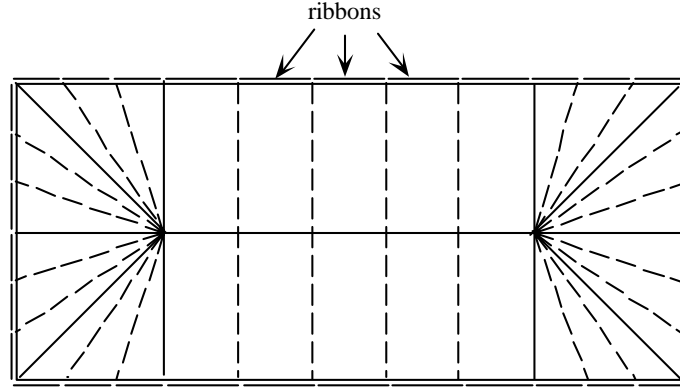


Figure 2.9): Segmentation scheme for a rectangular conductor for EII approximations.

The first step of calculating series impedance using the SRM is determining the number of surface ribbons used for conductor i , N_i , in the simulation. This number can be as small as four for a rectangular conductor and needs to be increased for higher accuracy. Once this number is determined, each conductor perimeter is divided into N_i segments, which are called surface ribbons, and each conductor cross-section is divided into N_i sections whose shapes are triangular, rectangular, or trapezoidal. The typical segmentation scheme for a rectangular conductor was introduced in the previous section and is shown in figure 2.9. The surface impedance of each segment is calculated for each section using either (2.22) or (2.23). The k^{th} diagonal term of $[Z_{eii}]$ can be determined using averaged surface impedance,

$$Z_{eii}^k \approx \frac{Z_s}{w_k}, \quad (2.24)$$

where w_k is the width of the k^{th} ribbon and Z_s is the surface impedance calculated using (2.22) or (2.23) for the k^{th} section that shares one side with the k^{th} ribbon. The elements of dense matrix $[L]$, the self and mutual inductance of ribbons, are calculated either carrying out direct numerical integration of the second term of (2.15) or using analytical equations [5]. Then for a given voltage setup, current flowing in each ribbon is calculated. Equation (2.16) is formulated for partial series impedance and the dimensions of the matrices are $N \times N$, where N is the total number of ribbons used. This matrix has to be converted into $N_s \times N_s$, where N_s is the number of signal conductors, to apply the SRM to the transmission line analysis. This can be done through nodal analysis or a mesh-based approach [6, 7]. The voltage and current vectors in (2.15) are the branch vectors and should be converted into nodal vectors. In nodal analysis, this can be done through

$$\begin{bmatrix} Z & -A^T \\ A & 0 \end{bmatrix} \begin{bmatrix} I_b \\ V_n \end{bmatrix} = \begin{bmatrix} 0 \\ I_s \end{bmatrix} \quad (2.25)$$

where $[I_s]$ is a source current vector, $[Z] = [Z_{eii}] + j\omega[L]$, $[I_b]$ is a branch current vector shown in (2.15), and $[A]$ is an incident matrix which relates node voltage and current vectors with

$$[V_n] = \{ [A][Z]^{-1}[A]^T \}^{-1} [I_n] \quad (2.26)$$

As an example, a two rectangular conductor case is analyzed. Both the TLM and the PWM results are shown in figure 2.10 compare well to the VFM result. For the SRM, 40 ribbons are used, while 1575 filaments are used for the VFM at 10GHz. For the SRM, the segmentation scheme shown in figure 2.6 is used. The maximum error of inductance calculation is 1.5% for PWM and 2.5% for the TLM. The maximum error of resistance calculation occurs near 10GHz, about 4% for the TLM and the PWM.

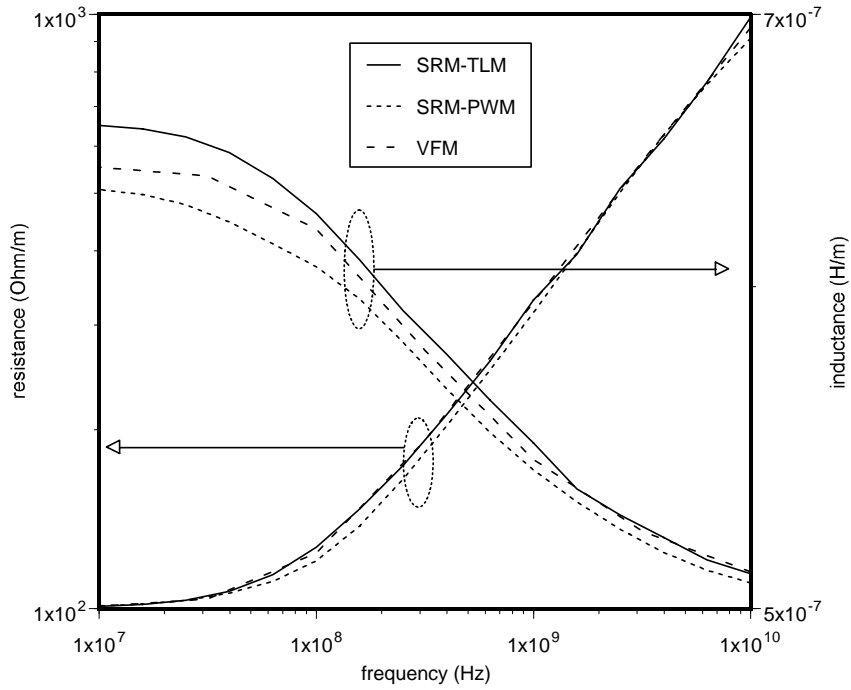
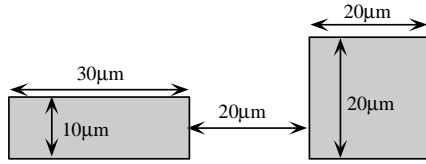


Figure 2.10) Series impedance of two asymmetric rectangular conductors. Comparison between the VFM and the SRM.

2.5.2 Arbitrary Cross-sectional Conductor

The SRM has been successfully applied to circular and rectangular cross-sectional shaped conductors [10, 11]. The extension of the SRM to conductors beyond these geometries is possible using the TLM. In this section, the SRM is applied to arbitrary cross sectional conductors. There are a few ground rules of discretization. First, the shape of the elements should be triangular, rectangular, or trapezoidal. This is because these are the cross-sections whose surface impedances can be approximated from (2.21) to (2.24); other shapes can be used if the surface impedance approximations for them are known. Second, two of the nodes of each element have to lie on the surface of the conductor such that the line connecting these two points coincides with the surface ribbon. This second restriction guarantees the number of ribbons used is the same as number of elements from the discretization. The third rule is the utilization of the symmetry of the conductor if there is any. For instance, for circular conductor shown in figure 2.4(a), many triangular elements are used and the internal node is chosen to be the center of the circle. This internal node is chosen such that all the triangles have the same height.

As an example, two trapezoidal shaped conductors are analyzed. Figure 2.11(a) shows three different segmentation schemes. The best segmentation should be able to minimize the number of ribbons without losing the accuracy. Among these three segmentations, the scheme 1 and 3 are useful when w_2/t is big, but if this is not the case, these schemes would require more ribbons to achieve the same accuracy as scheme 2. The scheme 2 is the best choice when w_2/t is small or when minimum number of ribbons is desired. As figure 2.11b shows, scheme 1 shows best inductance agreement, while scheme 2 is best for resistance calculation. In this particular case, w_2/t is too big to use scheme 2. Here, a total of 32 ribbons are used in all cases. The maximum resistance error for scheme 1 is 7.5% at 1GHz, 6% for scheme 2, and 1% for scheme 3, while the maximum inductance error for scheme 1 is 2%, 11% for scheme 2, and 7% for scheme 3, all occurring at low frequency.

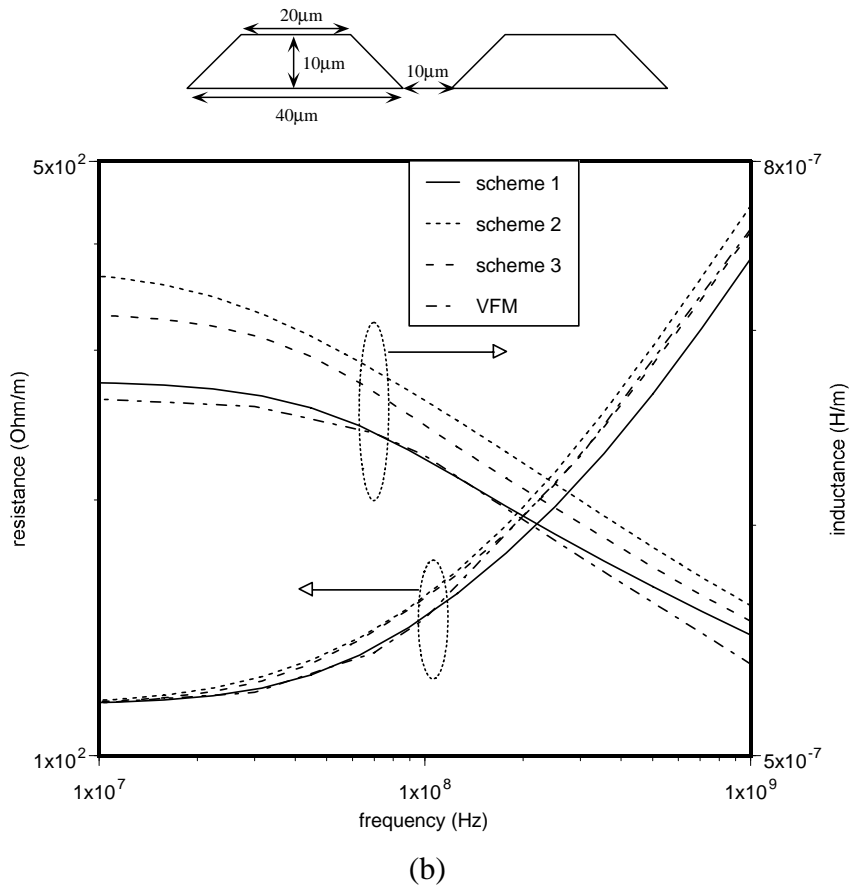
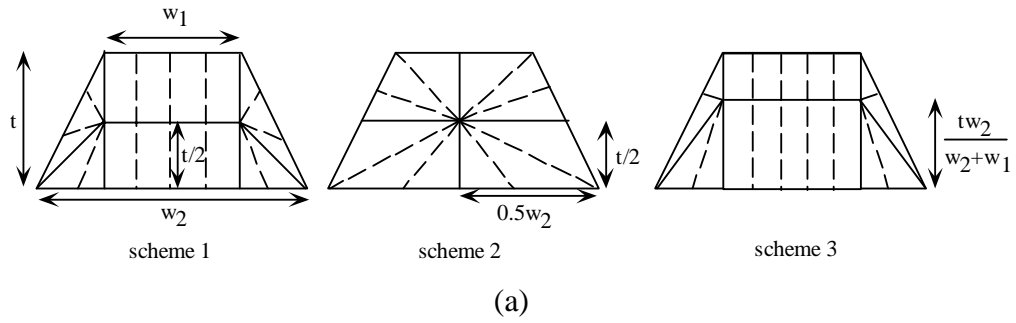


Figure 2.11: Three different schemes for the EII approximation of a trapezoid. (a) Three segmentation schemes. (b) Series impedance calculation of two trapezoids: Comparison to the VFM.

2.5.3 Minimization of Surface Ribbons

To achieve a greater accuracy, many ribbons have to be used in SRM. However, it would be interesting to investigate the trade-off between the accuracy and the number of ribbons used. Because of the nature of the dense inductance matrix, it is difficult to improve the computation time for inverting a large matrix. This is because an iteration matrix inversion method can not improve computation time significantly compare to direct inversion methods when the matrix is dense, and simply ignoring small matrix elements can generate an ill-conditioned matrix. Therefore, it is important to reduce the matrix size at the beginning, which is why SRM can be useful. The minimum segmentation method has been successfully applied to the SRM to reduce the matrix size [28]. In this section, error estimation for this technique is performed in comparison to the VFM. Also, the reason why this technique works better for certain cases than others will be explained. As was explored in the section 2.3, the EII has localized characteristics. This allows the effective separation of the skin effect and the proximity effect when we analyze the frequency dependent characteristics of multi-conductor transmission lines; The skin effect is analyzed through the EII while the proximity effect is taken care of through calculating mutual inductances between surface ribbons. As the frequency of interest becomes higher, the dominant effect is due to the skin effect. Therefore, the problem size can be significantly reduced by under-analyzing the proximity effect (use a very small number of surface ribbons). This technique should work fine whenever the proximity effect is insignificant.

For a rectangular conductor, four ribbons are used, i.e. one ribbon per side. The segmentation is done such that a rectangular conductor is divided into two triangles and two trapezoids. For a wide ground plane, rather than assigning ribbons along the four perimeters, only the side where the ground plane faces the signal lines is segmented. One ribbon is used right underneath the signal conductor with the same width as signal conductor, then besides this center ribbon, two ribbons with

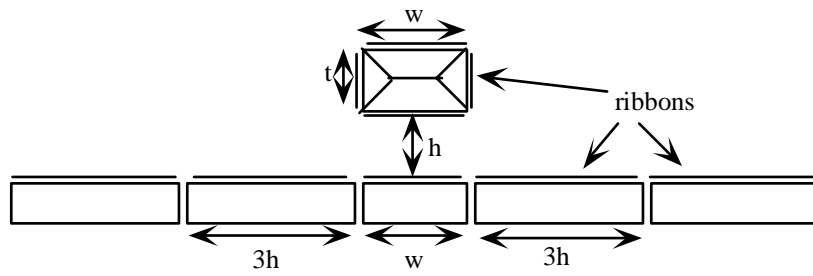
width $3h$ are used. This scheme is illustrated in Figure 2.12a where a total nine ribbons are used including the ground plane. The ground plane surface impedance can be calculated from (2.22) by replacing $t/2$ with t , while the surface impedance of trapezoidal section is

$$Z_s = -j \sqrt{\frac{j\omega\mu}{\sigma}} \frac{H_1^{(1)}(a)H_0^{(2)}(b) - H_1^{(2)}(a)H_0^{(1)}(b)}{H_1^{(1)}(b)H_1^{(2)}(a) - H_1^{(1)}(a)H_1^{(2)}(b)}, \quad (2.27)$$

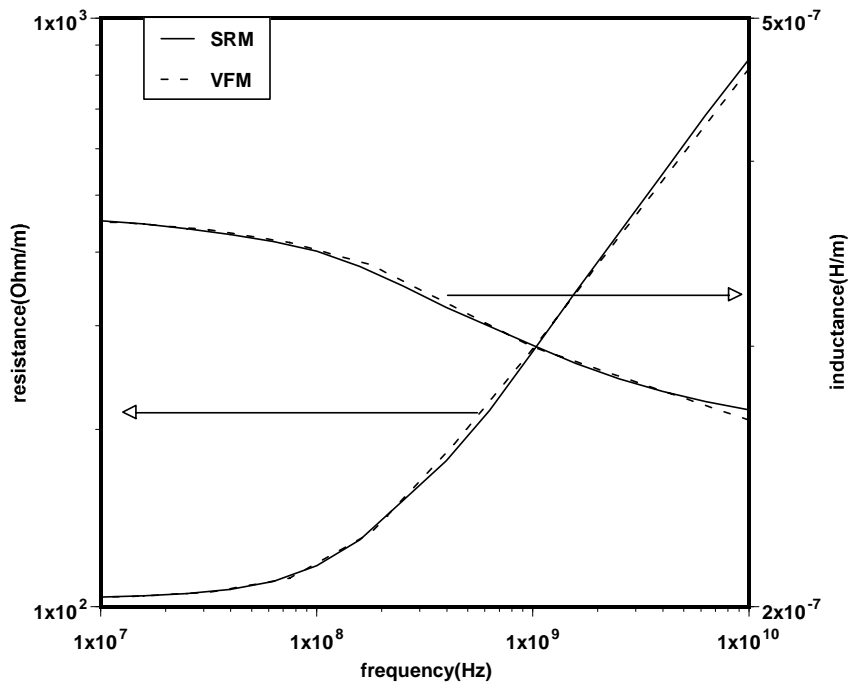
where $a = \frac{tw_1 \sqrt{-j\omega\mu\sigma}}{w_2 - w_1}$, $b = \frac{tw_2 \sqrt{-j\omega\mu\sigma}}{w_2 - w_1}$, and $H^{(1)}$ and $H^{(2)}$ are Hankel

functions of the first and second kind respectively. Figure 2.12 shows the comparison between the SRM using 9 ribbons throughout the frequency range and the VFM that requires 2290 filaments at 10GHz. 20 frequency samples are obtained within a second for the SRM calculation with 266MHz Pentium II.

Figure 2.13 shows the maximum error estimated from DC to skin effect high frequency (frequency at which the skin effect is dominating) calculated in comparison with the VFM. Generally the maximum error occurs at mid frequency range (frequency where proximity effect are influencing series impedance). The error curve indicates, this minimum ribbon scheme can estimate series impedance accurately for wide range of geometry. For more accurate result, the number of ribbons used has to be raised. The error becomes big when conductors are wide (see Figure 2.13). This is because the current re-distribution inside of the conductor is dramatic when conductors are wide and close to each other.



(a)



(b)

Figure 2.12: Minimum segmentation method. (a) Segmentation and ribbon assignment for a signal line above a wide ground plane. (b) Series impedance calculation using minimum segmentation method. $W=20\mu\text{m}$, $t=10\mu\text{m}$, $h=10\mu\text{m}$, ground plane width= $100\mu\text{m}$, ground plane thickness= $10\mu\text{m}$.

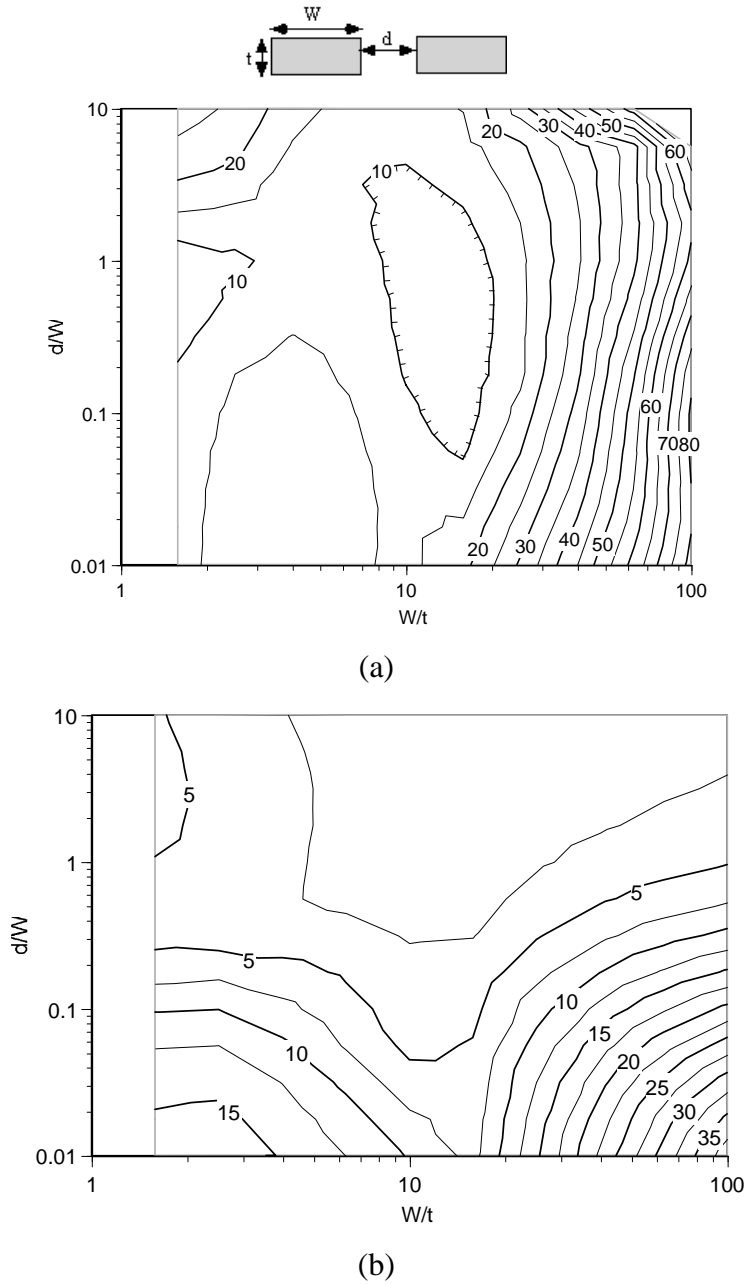
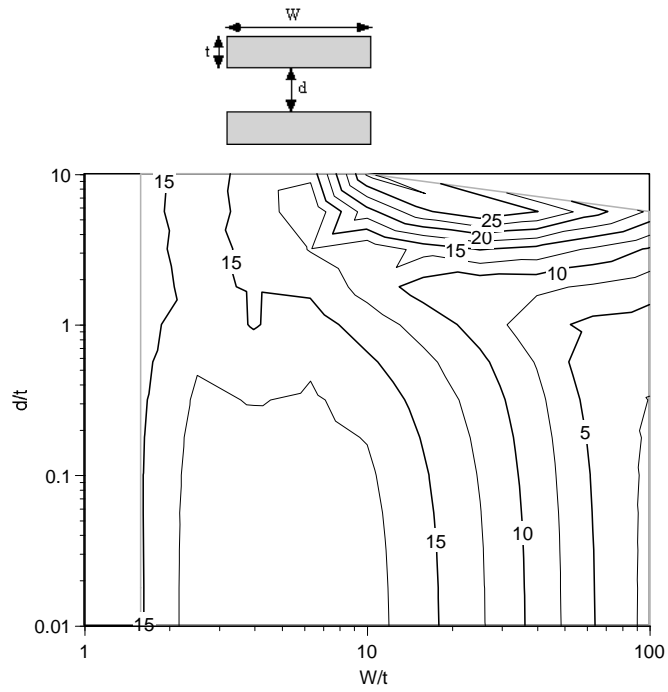
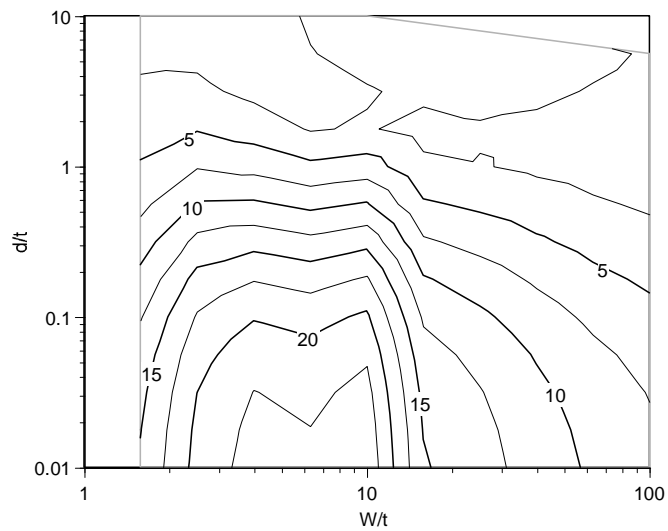


Figure 2.13: Maximum local error for the two symmetric conductors. (a) Resistance and (b) Inductance error estimation of the SRM using minimum segmentation: Comparison to the VFM. Error is estimated from DC to frequency where the thickness is 10-skin depth.



(a)



(b)

Figure 2.13: Maximum local error for two symmetric conductors (a) Resistance and (b) Inductance error estimation of the SRM using minimum segmentation:

Comparison to the VFM. Error is estimated from DC to frequency where the thickness is 10·skin depth.

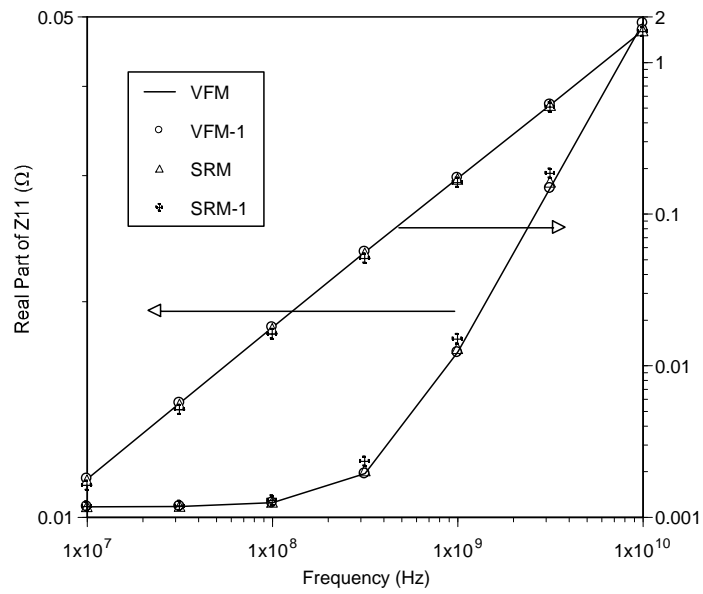
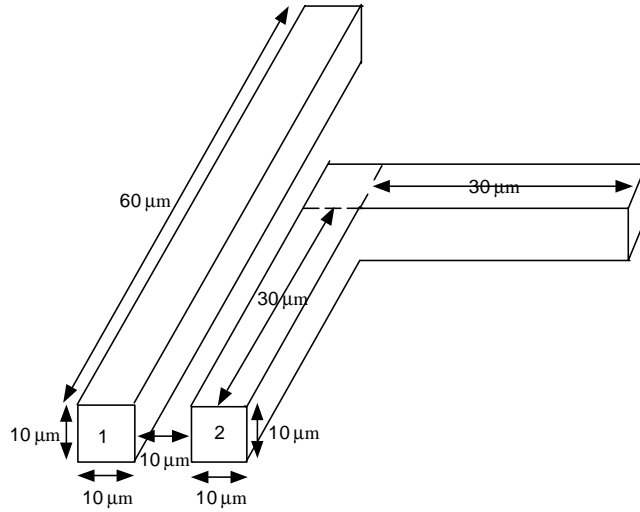
2.5.4 Three-dimensional Geometry

The analysis of 3-dimensional structures such as clock distribution network, vias, meshed ground planes, and I/O pin networks is becoming more important and difficult as technology advances since the structure becomes electrically small as the device speed goes up. The current distribution near the corners is extremely non-uniform and all three directional currents (x, y, z directions in cartesian coordinates) have to be modeled to accurately estimate series impedance. The SRM has been successfully applied to 3-dimensional structures [10], and is much more efficient than the widely used the PEEC [14]. However, as long as the discontinuity of the structure is not a dominant portion of the overall structure, the problem can be further simplified by assuming a current flows only in the length direction (this is often called $2\frac{1}{2}$ dimensional solution). In this section, $2\frac{1}{2}$ dimensional SRM is applied to the 3 dimensional structure. This solution technique is accurate if discontinuity inductance is much smaller than total inductance,

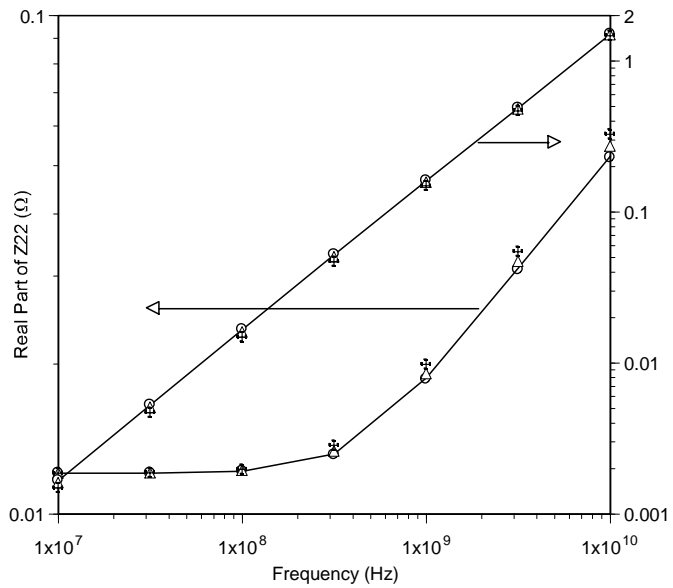
$$L_{discontinuity} = L_{total} - L_{uniform} . \quad (2.25)$$

where $L_{uniform}$ is the inductance obtained through a $2\frac{1}{2}$ dimensional solution. Figure 15(a) shows the example case of 3 dimensional structure often found in a clock distribution network. The partial inductances of these two lines are calculated using VFM and SRM. First, each line is divided into 9 segments in the length direction. For VFM, 15 filaments are used in width and thickness directions resulting in 225 filaments in cross-sectional area and 4050 filaments overall. For SRM, the same number of ribbons are used in the width, thickness, and length direction, resulting in 1080 ribbons overall. The results show good agreement. To minimize the matrix size, only 1 section can be used in length direction (2 sections for bend structure) without losing the accuracy. This approximation will reduce the overall number of filaments and ribbons to 675 and 180 respectively. In addition, for SRM, no more

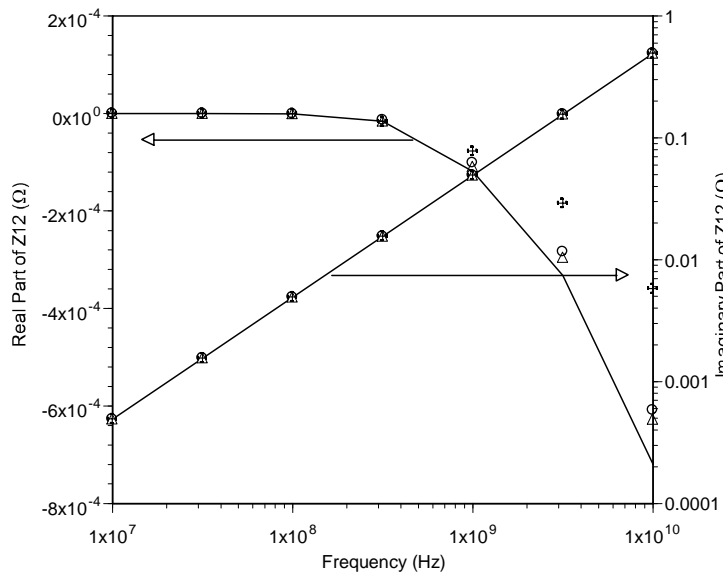
than 5 ribbons per side (total 60 ribbons) would be necessary to achieve a good agreement (see Figure 2.15(b)-(d)).



(a)



(b)



(c)

Figure 2.15): Series impedance calculation of three-dimensional structure using the SRM: Comparison to the VFM. (VFM: VFM using 9 segmentations along the length direction, VFM-1: VFM using 1 segmentation along the length, SRM: SRM

using 9 segmentations along the length direction, SRM-1: SRM using 1 segmentation along the length direction). (a)Z11, (b)Z22, (c)Z12.

2.6 Discussions

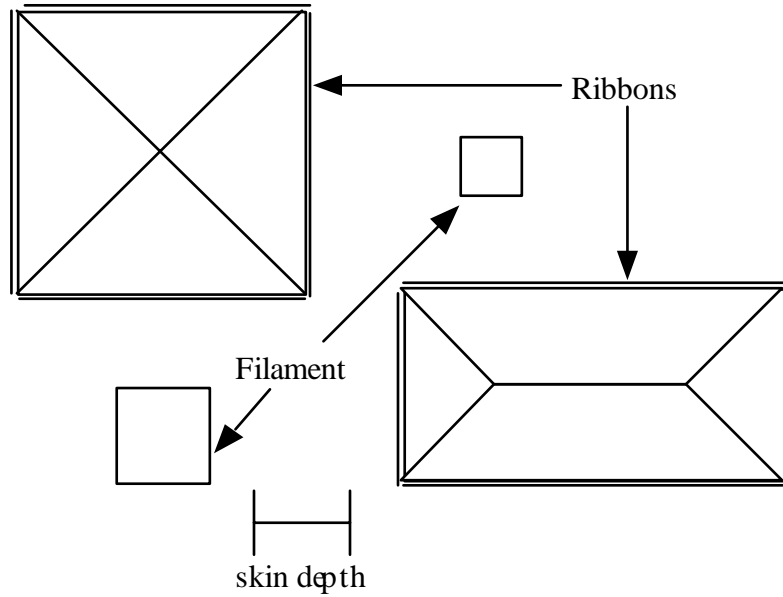


Figure 2.16): Combination of the SRM and the VFM in multi-conductor environment.

The advantages of the SRM in terms of memory and CPU time can be enormous when multiple conductors are simulated simultaneously and the highest frequency interested is in skin effect range. For square conductors, assuming the segmentation is done such that the dimension (ribbon width or filament width) is the same as a skin depth, the matrix dimension that has to be inverted for the VFM would be mN^2 , while it would be $4mN$ for the SRM, where m is number of conductors and $N \approx \text{width of the conductor} / \text{skin depth}$. In addition, the minimum segmentation scheme introduced in 2.5.3 can reduce the dimension of matrix to $4m$, which will lower the CPU time and memory usage by tremendous amount without sacrificing the accuracy. Considering the matrix is dense for both cases, the inversion

cost is proportional to M^3 , where M is the dimension of the matrix. Further study is needed for iteration inversion technique using efficient pre-conditioner.

Finally, when multiple conductors are simulated and the dimensions of the conductors are wide spread, the VFM and the SRM can be used together to reduce the matrix dimension. For instance, when the conductor dimension is less than a skin depth, a single filament can represent this conductor, while if this is not the case, SRM with four ribbons is used. This technique is illustrated in figure 2.16. Other applications of the SRM are series impedance calculation of the conductors coated with other conductor materials with different conductivity, planar inductors with significant loss factor, and planar resonators, etc.

Because most of the parameters including inductance can be calculated using analytical expressions (see Appendix A), the most time consuming part of the SRM simulation is due to the matrix inversion. The inductance matrix resulting from the SRM or the VFM are partial inductance, which makes an iteration inversion scheme much more difficult. In [29], a sparse inductance matrix is generated by shifting the matrix using new partial inductance concept. In this technique, the current is assumed to be returning at an arbitrary distance, which is different from the general partial inductance concept, therefore, mutual inductance outside of this fictitious returning sphere becomes zero. This method avoids an ill-conditioned matrix, which often resulted from other techniques that simply eliminate low magnitude matrix elements. This method is similar to the capacitance extraction scheme that utilizes a fictitious widow outside which all the conductors are ignored. By using this method, tremendous amount of matrix elements can be assumed to be zero, resulting in a sparse matrix which can be much more effectively solved using an iteration method such as the generalized minimum residual method (GMRES, [30]). However, when lines are lossy or the frequency of interest is low compared to the dimension of the conductor (i.e., on-chip interconnects), a significant amount of current might return through conductors outside of the window. This is because the current is bound to

flow through low resistance conductors even if they are far away from the signal lines.

Other iteration techniques using pre-conditioners have been developed to accelerate the matrix solutions. The typical preconditioning methods are local inversion and preconditioning using diagonal elements of the inductance matrix. The efficiency of these techniques depends on the convergence of the residuals. Also, the multipole algorithm introduced in [7] for the VFM can be also applied to the SRM to accelerate the simulation further [31]. The non-uniform segmentation technique applied in the VFM, which uses smaller filaments near the corners, can also be helpful for SRM since the current distribution on rectangular conductor at high frequency is similar to the charge distribution on perfect conductor [8].

2.7. Conclusions

In this chapter, the theoretical bases for the EII and the SRM are introduced. The surface equivalence theorem is applied to the original problem to derive the EII. The unique characteristics of the EII are observed, which can be very useful for the series impedance extraction. The SRM is based on the surface integral equations implementing the EII and effectively analyze skin effect and the proximity effect separately. Therefore the multi-conductor transmission lines can be easily analyzed through this technique. Also, reduction of the problem is possible with very little accuracy loss. The SRM has been applied to arbitrary cross-sectional conductors as well as three-dimensional structures.

Chapter 3

Time Domain Simulation Technique Using SPICE Circuit Model

The technique based on the equivalent circuit that models frequency dependent characteristics of the transmission lines [5, 16-18, 32] can be numerically expensive mainly because the number of the nodes involved becomes large especially when the rise time of the input becomes short. However, this technique is still a widely used method due to its flexibility with various simulators. Also, most on-chip interconnects are modeled through this technique since the cross-sectional dimension is small and the length of the lines is short.

The circuit model based on the VFM [5, 18] can be impractical due to the large number of nodes, while the other techniques based on simple model [17] are not accurate. For the equivalent circuit modeling to work well in time domain simulation it should match the frequency response accurately. To accurately model a transmission line in wide frequency range, skin effect as well as proximity effect has to be predicted in a circuit model. Wheeler [33] introduced uniform lumping into transverse direction to capture the skin effect, however, the number of the lumps has to be minimized to simulate efficiently. Yen [17] reduced the number of lumps used significantly, but no clear rule for choosing values of the elements were given. In [16], compact circuit model consists of 3 inductors and 4 resistors was developed to predict skin effect (Fig 3.1). However, this method has a difficulty in modeling rectangular conductors. In this chapter, first, delay estimation of the on-chip interconnects will be performed using RC lines. Then RLC circuit will be introduced to model frequency dependent multi-conductor transmission lines with arbitrary cross-section.

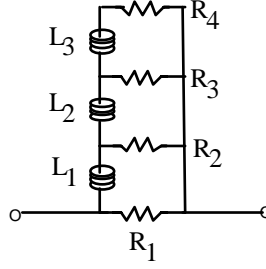


Figure 3.1): Equivalent RL ladder circuit model for the skin effect.

3.1 RC Delay Estimation for the On-chip Interconnects

When the conductor cross-sectional dimension is small compare to the skin depth, which is often the case for on-chip interconnect, it is useful to use analytical equations to estimate delays. Figure 3.2 shows four different types of the circuit model to represent a simple RC line. To derive a simple equation from these circuit models Elmore delay can be used. By using the first two moments of these circuit models, the Elmore delay can be determined [34]. Then the circuit impulse response would be $v(t) = 1 - e^{-t/T_d}$, where T_d is an Elmore delay.

Suppose total line resistance is R_t , total line capacitance is C_t , termination capacitance (or input capacitance of the receiver circuit) is C_L , and the source resistance (or internal resistance of the driver) is R_s . If the line is divided into n segments to model a distributed RC line, where n can be determined using

$$f_{\max} \leq \left| \frac{2n^2}{R_t C_t} \left(1 - \cos \frac{(2n-1)\pi}{2n} \right) \right|, \quad (3.1)$$

the Elmore delay for Pi or a T type model is

$$T_d = k_1 R_s (C_t + C_L) + k_1 R_t C_L + k_2 R_t C_t \quad (3.2)$$

where k_1 is 1 and k_2 is 0.5. For an R-C type model,

$$T_d = R_s (C_t + C_L) + R_t C_L + \frac{(n+1)R_t C_t}{2n}, \quad (3.3)$$

and for an C-R type model,

$$T_d = R_s(C_t + C_L) + R_t C_L + \frac{(n-1)R_t C_t}{2n}. \quad (3.4)$$

Note both (3.3) and (3.4) approaches (3.2) (with $k_1=1$, $k_2=0.5$) as n gets bigger. To apply these results to the actual delay estimation, 0.7 is multiplied to each parameters ($k_1=0.7$, $k_2= 0.35$) to account for the rise time effect [35]. In the empirically determined equations introduced in [36, 37], k_1 and k_2 are given as 0.7 and 0.4 respectively, while in [38], these parameters are a function of the rise time.

Figure 3.4 shows a comparison between the equations and simulation results. For the simulation results, two cases (figure 3.3) where the RC line is driven by a constant voltage source and by an actual CMOS inverter circuit are shown. For the constant voltage source, the source resistance is determined as $R_s = V_{dd} / I_{dd} - Z_0$, where V_{dd} is the power supply voltage, I_{dd} is the drain current of the inverter, and Z_0 is the characteristic impedance of the line. The most interesting aspect is that even though all the equations give quite accurate matches for a constant voltage source model, they overestimate delays comparing to the delay simulated from the actual inverter circuit. This discrepancy is due to the nature of the inverter circuit. Since the inverter circuit acts more like a constant current source rather than voltage source for a quite long duration, the constant voltage source cannot represent all the inverter behaviors. This difference can be observed by obtaining the current waveform at the input and output terminal as is shown in Figure 3.5. Because of this difficulty, it is desirable to simulate the actual waveform to accurately estimate the delays when an inverter circuit (or any other CMOS gates) is used as a driver circuit. The overestimation of the delays leads to conservative design, which can result in over-use of buffers, use of over-sized drivers, and increase of the die size.

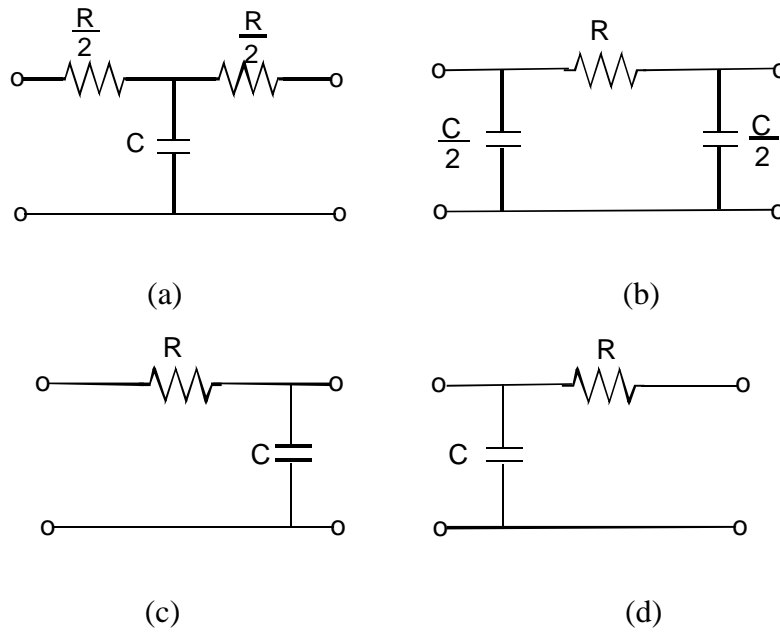


Figure 3.2): Typical RC lumped circuit models. (a) T model, (b) Pi model, (c) R-C model, (d) C-R model.

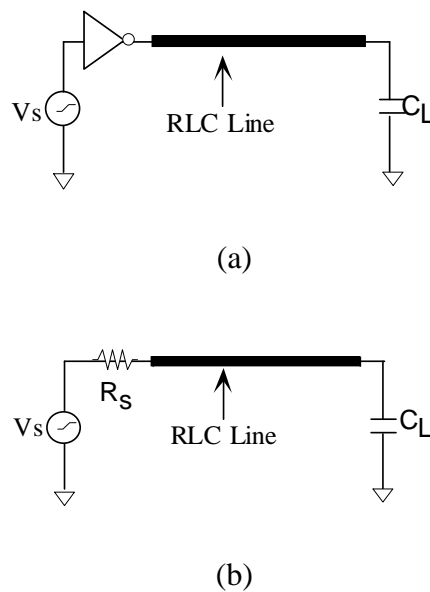
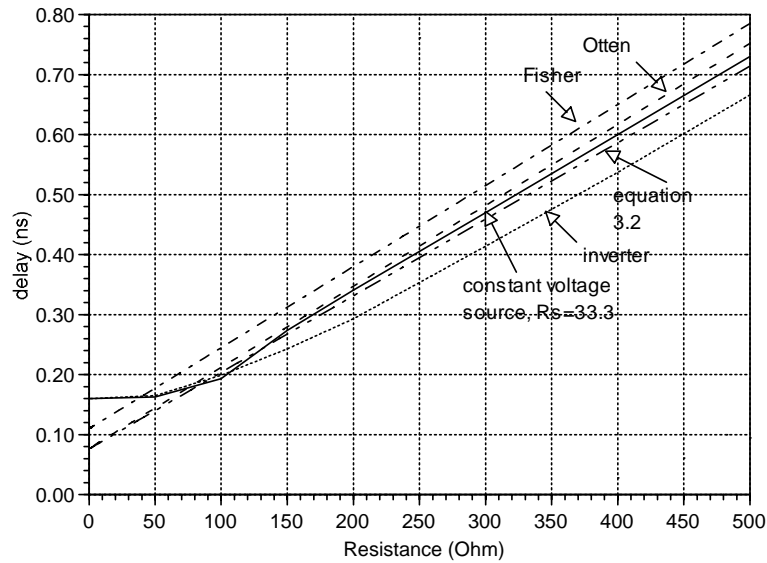
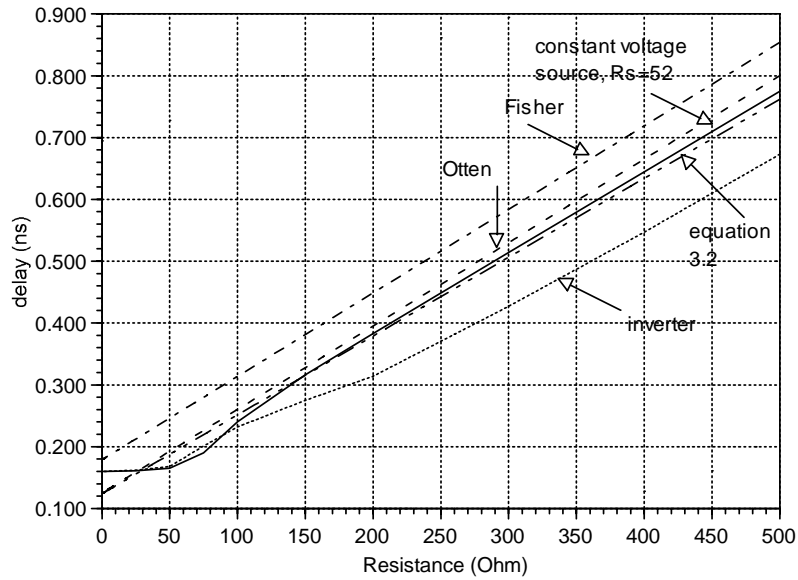


Figure 3.3): Global wires driven by the (a) inverter and (b) its equivalent circuit using constant voltage source and internal resistance.



(a)



(b)

Figure 3.4): Comparison of the delay estimation for 20mm line. (Inverter: Hspice simulation using inverter circuit, Constant voltage source: Hspice simulation using constant voltage source and an equivalent source resistance, Fisher: equation given in [37], Otten: equation given in [36]). (a) driver with 30mA current driving capability, (b) driver with 24mA current driving capability.

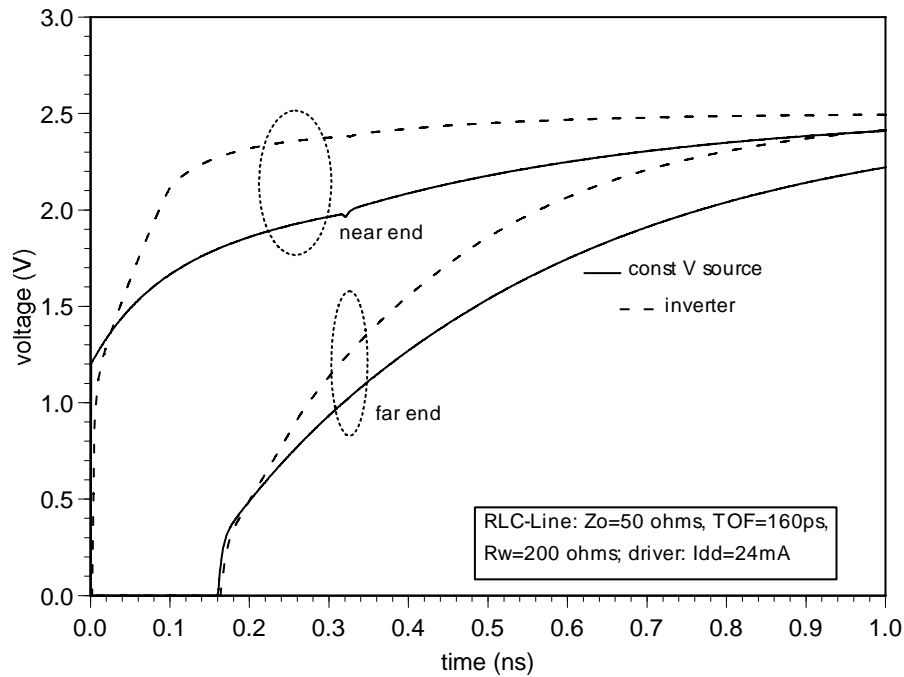


Figure 3.5): Near end and far end current waveform for the 20mm transmission line driven by the 24mA inverter and its equivalent circuit model.

3.2 Importance of the RLC Circuit Modeling

When the resistance does not dominate ωL , the inductance of the line has to be included in the circuit model. This could be true even for the on-chip interconnect that carries the signal relatively long distances. Most of these lines are the higher level metal lines and the cross-sectional dimensions of these lines are designed to be "fat" such that the line resistance does not effect the total delay. Despite the fact that the frequencies of interest are not high enough for the skin effect to be considered as a major factor in estimating delays (i.e. skin depth is bigger than the cross-sectional dimension), the appropriate inductance value has to be included in the circuit model. It has been reported that when line resistance is less than $2Z_0$, and/or when the source resistance is small compare to Z_0 , the inductance can impact the delays [4].

The crosstalk has become an important factor in design considerations, since as technology advances the line density needs to be increased. The number of the metal layers is limited not only because of the dramatic manufacturing cost increase but also because the blockage of the lines due to the vias becomes significant as the number of the metal layer increases. On the other hand, the thickness of the line is increasing continuously compared to the width of the line to reduce the resistance of the line without costing line density. The crosstalk problem in the lower metal layers is dominated by capacitance coupling and cross proximity of the silicon substrate as well as orthogonal lines in different layers can reduce the crosstalk to some degree. However, careful placement of the ground/power lines has to be done to reduce the crosstalk further. For instance, a typical configuration of the lower metal layers is shown in Figure 3.6 (a). An appropriate placement of the power/ground lines at metal layer 3 with respect to layer 1 would be putting a ground/power at the location shown in Figure 3.6 (b). The most important, yet challenging task here is obtaining accurate self and mutual capacitance for the circuit model since 3 dimensional extraction is required due to the orthogonal lines (i.e. metal layer 2). The extractions using field solvers such as finite element method [39], finite difference method [40, 41] and boundary element method [42, 43] cannot effectively extract parameters when multiple lines have to be included, while analytical methods or geometry based simulation can give erroneous results. The conditions that inductance coupling has to be included in the circuit model are similar to the conditions introduced for self inductance. That is when the line resistance and/or source resistance are comparable with the characteristic impedance of the line, the inductance coupling can impact the result, which might be quite different from the simple RC line analysis. Due to the large capacitance load, large drivers are used to drive the global wires. Also, these lines are designed to be “fat” to reduce the total delays. These design considerations push the limit of the exclusion of the inductance in the circuit model. Even though most on-chip interconnects have negligible inductance effects, erroneous results

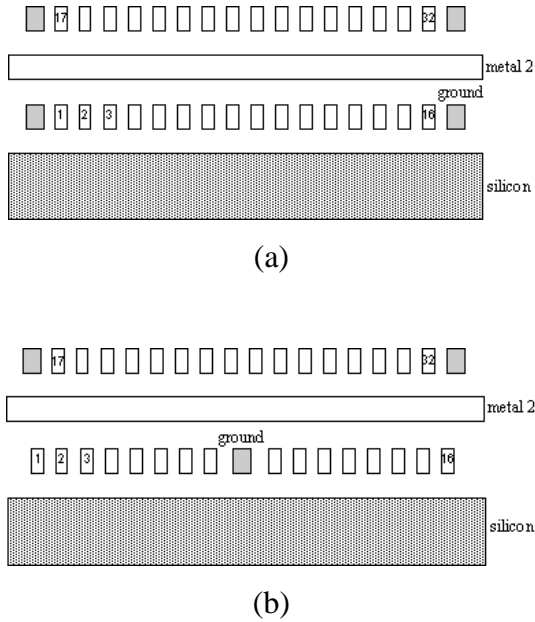


Figure 3.6): Configuration of the typical lower metal layers (Usually the dimension of the wires on level 3 is bigger than that of the wires in level 1).

from ignoring frequency dependency of the on-chip interconnects have been reported [4]. When package level lines are analyzed, the skin effect and proximity effect have to be included in the circuit model as the rise time of the signal gets shorter.

3.3 Compact Equivalent Circuit Model for the Skin Effect

At very high frequency, skin effect dominates proximity effect, and series resistance becomes proportional to square root of frequency. This square root dependency is fully developed when $f_{\min} \approx 5R_{dc}/L_{dc,tot}$ for most cases, although this frequency becomes higher when a conductor is wide, and geometrical proximity to a smaller line dominates. This square root dependency can be modeled with a compact circuit shown in figure 3.1 if the series impedance of the line at one arbitrary high frequency point (high enough so that the square root dependency is fully developed)) and at one low frequency point (close to DC) are known. This

high frequency series impedance, R_{high} and L_{high} , can be easily calculated using the SRM introduced in the previous chapter. Also, one low frequency series impedance, R_{dc} and $L_{dc,tot}$, can be calculated using the VFM with a single filament, which can be obtained using a closed form equation. For circular conductors, this ladder circuit model has been used to calculate the series impedance without the knowledge of two frequency points [16]. Here, the cross-section of the conductor is assumed to be arbitrary.

To determine the values of each element of the ladder circuit (Figure 3.1), all the elements are assumed to satisfy the following properties:

$$\begin{aligned} \frac{R_2}{R_1} = RR, \quad \frac{R_3}{R_2} = RR \cdot m, \quad \frac{R_4}{R_3} = RR \cdot m^2, \\ \frac{L_2}{L_1} = LL, \quad \frac{L_3}{L_2} = LL/m \end{aligned}, \quad (3.5)$$

where RR is a positive number smaller than 1, LL is a positive number bigger than 1, and m is bigger than 1 but less than 10; this parameter is additionally added to the original constraints given in [16] to capture geometrical proximity effect. However, this parameter can be fixed to 1 without much loss of accuracy for the symmetrical conductor cases. These three parameters (RR , LL , and m) are determined through an efficient optimization process that can be significantly simplified through the use of asymptotic approximations.

As a first step, this model has to give correct DC resistance since this is the most critical requirement for giving accurate time domain simulation. This restriction gives

$$R_1 = R_{dc} \frac{1 + (RR \cdot m^2) + m(RR \cdot m)^2 + (RR \cdot m)^3}{(RR \cdot m)^3}. \quad (3.6)$$

Through (3.6), R_1 can be found if RR and m are known. The next step is forcing the series resistance to be R_{max} at f_{max} , where

$$R_{\max} = R_{\text{high}} \sqrt{\frac{f_{\max}}{f_{\text{high}}}} \quad \text{and} \quad f_{\max} = 50 \frac{R_{dc}}{L_{dc,tot}}. \quad (3.7)$$

This requirement can be expressed through rough calculation by assuming that at f_{\max} all the currents flows through only first two "rungs" of the ladder circuit (R_1, L_1 , and R_2); this assumption gives

$$L_1 = \frac{1}{\omega_{\max}} \sqrt{\frac{R_1^2 (1 + RR)(R_1 RR - R_{\max} (1 + RR))}{(R_{\max} - R_1)}}. \quad (3.8)$$

Finally LL can be found by substituting (3.5), (3.6) and (3.8) in (3.9) and solving in terms of LL , giving

$$L_1 + \frac{R_2^2 \left[L_3 R_3^2 + L_2 (R_3 + R_4)^2 \right]}{\left[R_2 R_3 + R_2 R_4 + R_3 R_4 \right]} - L_{dc} \left[1 + \frac{R_2 R_3 R_4}{R_1 R_2 R_3 + R_1 R_2 R_4 + R_1 R_3 R_4} \right]^2 = 0, \quad (3.9)$$

where $L_{dc} = L_{dc,tot} - L_{\text{high}}$. This procedure is repeated until optimum combination of RR and m is found. Here, this optimum combination is determined such that it gives smallest local error in frequency range from f_{\min} to f_{\max} . Notice that there are bounds for RR and m to get a positive real number in (3.8). This requirement gives a restriction on RR and m :

$$\frac{1 + RR m^2 + RR^2 m^3 + RR^3 m^3}{RR^2 m^3 (1 + RR)} < \frac{R_{\max}}{R_{dc}} < 1 + \frac{1}{RR} + \frac{1}{RR^2 m} + \frac{1}{RR^3 m^3}. \quad (3.10)$$

This restriction gives additional efficiency in finding optimum RR and m , since they provide a smaller range that they can vary in. Also, the assumption that all the currents flow through only the first two rungs of the ladder at high frequencies allows one to predict the value of R_1 (or RR). The final model can be obtained by connecting L_{high} in series with the ladder in figure 3.1. This L_{high} represents external inductance at high frequency, while L_{dc} in (3.9) is internal inductance at low frequency. All the parameters determined (R_1, L_1, RR, LL, m) are independent of conductivity of the conductors as long as all the conductors have the same

conductivity, since the low and high frequency limiting values of inductance do not vary with conductivity.

Compact circuit models have been obtained by above procedure and compared with the surface ribbon method. Fig 3.7-3.9 shows three different cases. The first two cases (Fig 3.7 and 3.8) are symmetrical conductor examples, and not only local error but average error is very small. Next, micro-strip line (Fig 3.9) is tested, and maximum local error under 25% has been achieved. Table 3.1 shows the results of various geometries with different aspect ratio (width/thickness). To illustrate the advantage of introducing the additional parameter ' m ' the $m=1$ case is also shown. In this table, for coplanar type and parallel type conductors, the worst error among various spacing is chosen, while for micro strip lines, the worst error among various ground plane widths is chosen and height above ground plane is determined such that characteristic resistance is 50 ohm with dielectric constant 2.5. Further study shows that as the conductor width and thickness ratio gets bigger and as asymmetry between conductors gets more severe, the error becomes bigger. The biggest error in these cases appears near the transition frequency region where the skin effect is not fully developed. Figure 3.10 shows time domain waveforms of two signal lines above a finite conductivity ground plane. This waveform is compared to an FFT calculation using a full dispersion curve [44]. Since the model introduced here can be used as long as square root dependency of series resistance is obeyed, other multi-conductor simulation schemes can also be easily applied to this model. However, limited accuracy for asymmetric conductors and the requirement of pre-known series impedance at two frequency points make this approach unattractive. However, for time domain simulation purpose, the inaccuracy of this circuit model can be insignificant. In the following section, an equivalent circuit representation of SRM will be introduced.

Conductor Aspect Ratio (width/thick)	Coplanar Type Error(%)		Parallel Type Error(%)		Micro Strip Type Error(%)	
	m=1	1<m<10	m=1	1<m<10	m=1	1<m<10
1	15	17	15	17	21	21
5	25	20	25	22	55	25
10	23	15	30	22	50	20
20	36	18	30	25	41	25

Table 3.1) Maximum error for the equivalent circuit model (Always longer side is considered as width).

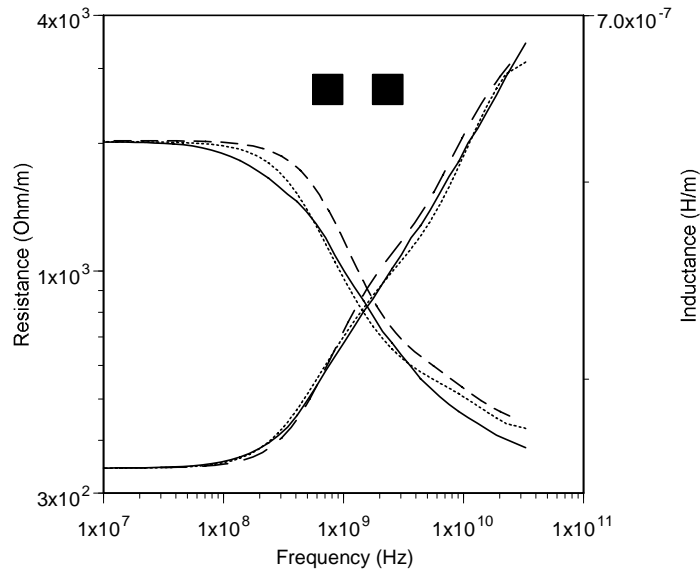


Figure 3.7) Two $10 \times 10 \mu\text{m}$ conductors with $10 \mu\text{m}$ separation. Solid line: Surface ribbon method, Dotted line: Circuit model using $m=2.1$, Dashed line: Circuit model using $m=1$. For $m=2.1$, $RR=0.339$, $LL=3.787$, $f_{\text{min}}=3\text{GHz}$, $f_{\text{max}}=30\text{GHz}$.

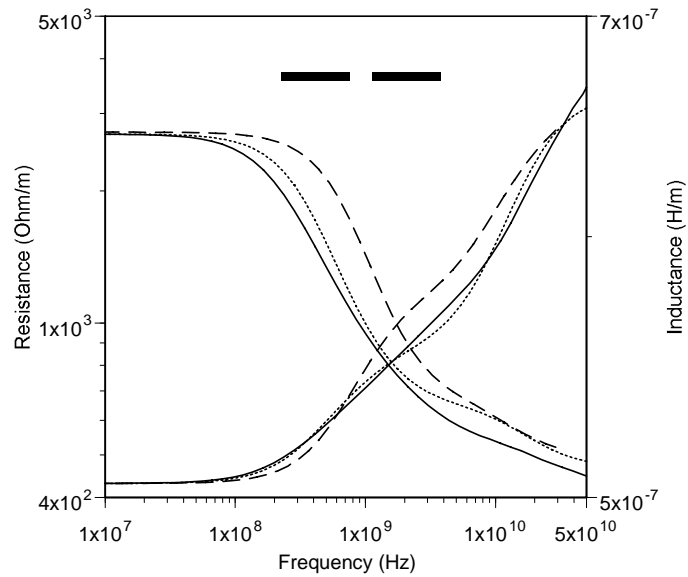


Figure 3.8): Two $40 \times 2 \mu\text{m}$ conductors with $10 \mu\text{m}$ separation. Solid line: Surface ribbon method, Dotted line: Circuit model with $m=3.1$, Dashed line: Circuit model with $m=1$, For $m=3.1$, $RR=0.325$, $LL=8.8$, $f_{\text{min}}=3.5\text{GHz}$, $f_{\text{max}}=35\text{GHz}$.

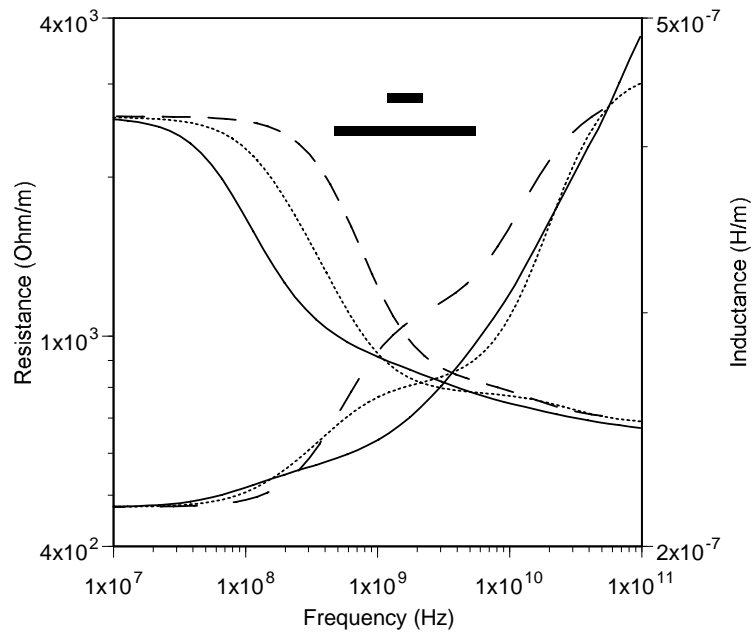


Figure 3.9): Strip line with signal line $20 \times 2 \mu\text{m}$ bar $8 \mu\text{m}$ above ground plane ($200 \times 2 \mu\text{m}$). Solid line: Surface ribbon method, Dotted line: Circuit model with $m=3.8$, Dashed line: Circuit model with $m=1$. For $m=3.8$, $RR=0.339$, $LL=30.6$, $f_{\text{min}}=6\text{GHz}$, $f_{\text{max}}=60\text{GHz}$.

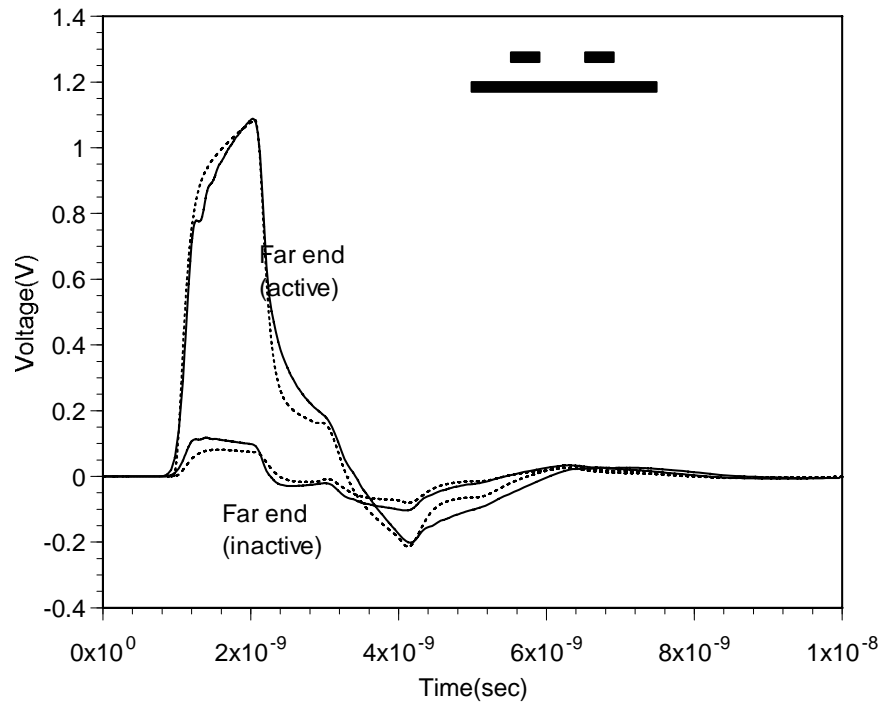
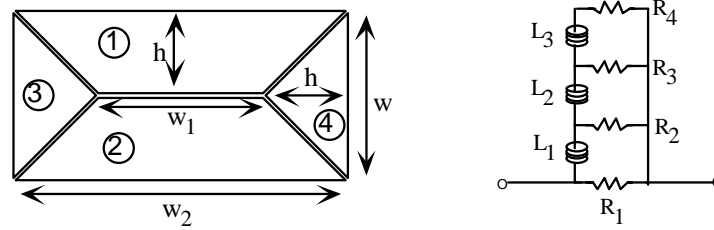
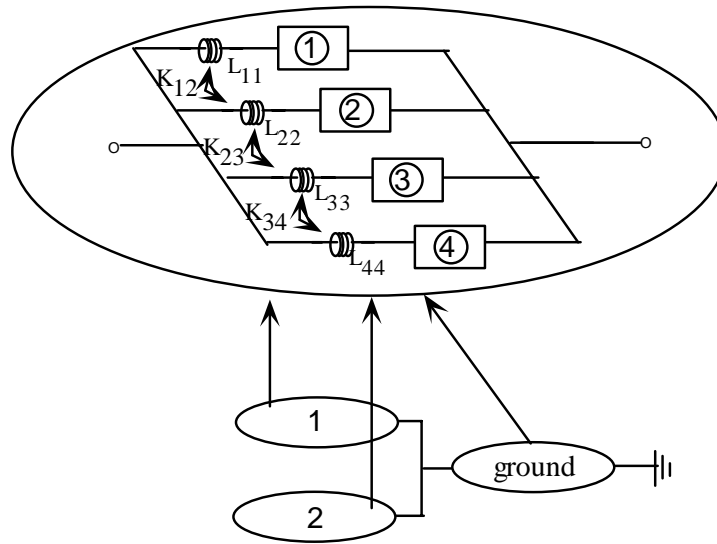
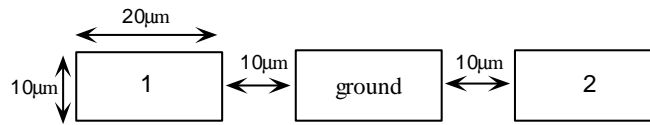


Figure 3.10): Two lossy signal lines ($8 \times 4 \mu\text{m}$) $12 \mu\text{m}$ above an imperfect ground plane ($200 \times 4 \mu\text{m}$). Separation between two conductors is $12 \mu\text{m}$. Rise and fall time = 0.1 ns , Terminations are capacitive (1 pF) with unmatched source resistance (10Ω). Solid line: Circuit model, dotted line: FFT.

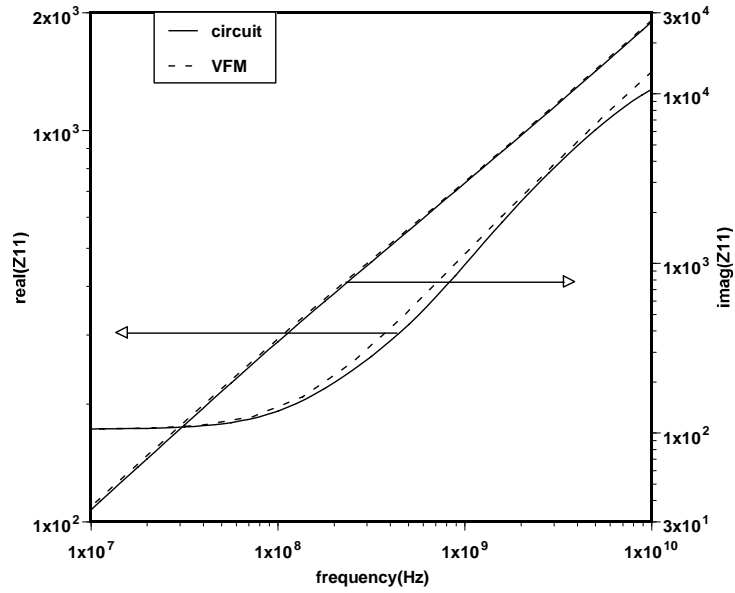


(a)

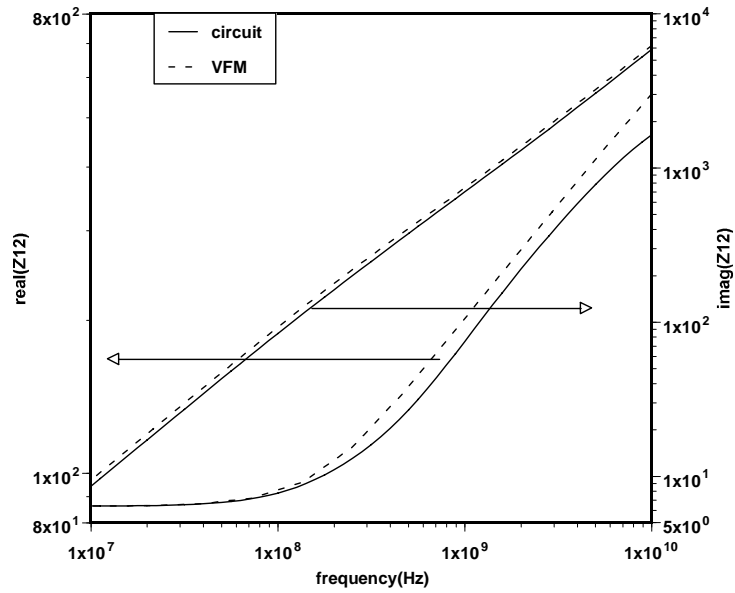


(b)

Figure 3.11: Equivalent circuit modeling using frequency independent circuit elements to capture frequency dependent characteristics of multi-transmission lines. (a) Segmentation scheme for a rectangular conductor and an equivalent ladder circuit model for each section to capture the skin effect (a ladder circuit models each subsection). (b) An example of the circuit model. An equivalent circuit model for the coplanar type conductors (Two signal lines and one ground line): Each numbered box represent a ladder circuit.



(a)



(b)

Figure 3.12): Series impedance calculation of coplanar lines (Figure 3.11(b)) using an equivalent circuit model: Comparison to the VFM. (a) Z_{11} , (b) Z_{12} .

3.4 RL Ladder Model for the SRM

To apply the SRM to the time domain simulation, equation (2.11) can be transformed into the time domain, which requires a transient form of the surface impedance. An efficient and stable method without going through numerical approximation is the RL ladder circuit model representation shown in figure 3.1. Similar approaches, which use numerical approximation methods rather than a circuit model, are reported in scattering problems [45, 46]. However, these approaches are not appropriate for transmission line problems where low frequency responses might be important.

For rectangular conductors, the conductor interior is divided into two triangles and two trapezoids as shown in figure 3.11, then an equivalent ladder circuit is used to represent each section. The approximations of the surface impedance of the trapezoid and triangle in the frequency domain are given in chapter 2 (equation 2.20 and 2.24). In an equivalent circuit, the RL ladder model shown in figure 3.11, which corresponds to each diagonal element of the matrix $[Z_{eii}]$ in (2.11), is connected in series with a self inductance, which corresponds to each diagonal element of the matrix $[L]$ in (2.11). Then four sections that belong to the same conductor are connected in parallel. Finally the complete circuit model can be constructed by including mutual inductances using off-diagonal terms of $[L]$.

The values of the RL ladder model can be easily determined with simple rules. First, two adjacent resistances and inductances in the RL ladder are related by

$$\frac{R_i}{R_{i+1}} = RR, \quad i = 1, 2, 3, \quad \frac{L_i}{L_{i+1}} = LL, \quad i = 1, 2, \quad (3.11)$$

where RR and LL are constants to be determined. Requiring the correct dc resistance and inductance to the EII yields

$$RR^3 + RR^2 + RR + (1 - \alpha_R) = 0, \quad \text{with } \alpha_R = C_1 \frac{P}{\delta_{\max}}, \quad \delta_{\max} = \sqrt{\frac{1}{\pi f_{\max} \mu \sigma}}, \quad (3.12)$$

and

$$\left(\frac{1}{LL}\right)^2 + \left(1 + \frac{1}{RR}\right)^2 \frac{1}{LL} + \left(\left[\frac{1}{RR}\right]^2 + \frac{1}{RR} + 1\right)^2 - \alpha_L \left(\left[1 + \frac{1}{RR}\right] \left[\left\{\frac{1}{RR}\right\}^2 + 1\right]\right)^2 = 0, \quad (3.13)$$

where $\alpha_L = C_2 \alpha_R$, f_{\max} is the highest frequency of interest depending on the rise time of the input signal, e.g. $f_{\max} \approx 1/T_{rise}$, and p is the conductor depth parameter shown in table 3.2. Here, C_1 and C_2 are constants unique to the geometry of the conductor and are shown in table 1. From (6), RR can be obtained for given geometry, then (3.13) can be used to obtain LL . Finally, each element value can be calculated through (3.11) and (3.14).

$$R_1 = \alpha_R R_{dc}, \quad L_1 = \frac{L_{dc}}{\alpha_L}, \quad (3.14)$$

where R_{dc} and L_{dc} can be calculated from closed form equations of surface impedance of an isolated conductor, e.g., for a circular conductor, $R_{dc} = \text{Re}(Z_{cir}(0)/w)$ (Z_{cir} is given by 2.17) and

$$L_{dc} = \frac{\text{Im}(Z_{cir}(f_{low})/w)}{2\pi f_{low}} \text{ where } f_{low} \text{ is arbitrary low frequency.}$$

To test the accuracy of the circuit model, the frequency dependent series impedance of coplanar type conductors has been calculated. Each rectangular conductor is divided into four sections, two trapezoids and two triangles, then table 3.2 and (3.11)-(3.14) are used to construct skin effect RL circuit model for each section. The equivalent circuit of this example is shown in Figure 3.11(b). Here, the direction of the self-inductance connections in ground return has to be the opposite of the self-inductance connections in signal conductors. Figure 3.12 indicates the circuit model simulated with Hspice [47] in frequency domain gives a quite accurate match compared to the volume filament technique. To improve the accuracy further, more than four ribbons and EII's have to be used for a signal conductor. However,

this is rarely necessary for time domain simulation. This equivalent circuit can be directly used in SPICE and since the values of the elements of the equivalent circuit can be obtained for a given geometry quite easily, computation time to extract frequency dependent parameters can be eliminated.

Geometry	p	C ₁	C ₂
Circular	Radius (r)	0.53	0.315
plate	Thickness (t)	10.8	0.2
Triangle	Height (h)	1.7	0.27
Trapezoid ($w_2/h < 10$)	Height (h)	w_2/h	0.3
Trapezoid ($w_2/h > 10$)	Height (h)	11	0.3

Table 3.2) Geometry dependent constants used in construction of an equivalent circuit.

3.5 Reduction of the Ladder Using a Single Pole

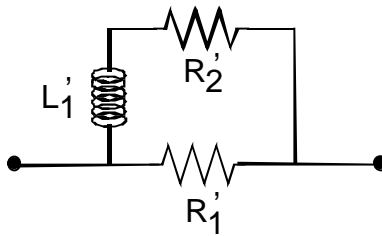


Figure 3.13): An equivalent circuit model of figure 3.1 using a single pole approximation.

The equivalent circuit (Figure 3.1) has three poles. However, as the number of conductors becomes large, a single dominant pole can be used to reduce the

computation time and memory usage. The original rational function and a reduced form of it are:

$$\frac{Z_{eii}}{s} = \frac{a_3s^3 + a_2s^2 + a_1s + a_0}{s(b_3s^3 + b_2s^2 + b_1s + b_0)} = \frac{k_1}{s} + \frac{k_2}{s + p_2} + \frac{k_3}{s + p_3} + \frac{k_4}{s + p_4} \approx \frac{k_1}{s} + \frac{K}{s + P} \quad (3.15)$$

where P is the dominant pole of p_2, p_3 , and p_4 . Here, the pole at $s=0$ is excluded from the one pole approximation since the $s=0$ pole “hides” the other poles. The reduced order model is now equivalent to a “two ladder” model shown in figure 3.13 with values given by

$$R_1' = k_1 + K, \quad R_2' = \frac{k_1}{K}(k_1 + K), \quad L_1' = \frac{(k_1 + K)^2}{|P \cdot K|} \quad (3.16)$$

In obtaining a single dominant pole in (3.15), the EII is divided by s to simplify the time domain equation of the SRM. The derivation of a time domain SRM equation will be covered in the next chapter.

3.6 Discussions

A compact equivalent circuit model whose elements can be easily determined using analytical equations has been developed. The study done in [4] suggest that when the source resistance and the series resistance are comparable to the characteristic impedance of the line, the frequency dependent series impedance has to be included in the circuit model. Further study shows that this might also be true when the line capacitance is much bigger than termination capacitance. Global wires are driven by a large inverter and terminated with small local device, which favors the necessity of RLC circuit model rather than an RC model.

The equivalent circuit model introduced in this chapter can be used when the skin effect and proximity effect are contributing to the time domain waveforms. The number of the elements involved in this equivalent model is much smaller than equivalent circuit for the VFM and PEEC [5, 14].

Chapter 4

Time Domain Simulation Technique Using the SRM

Despite the fact that numerous time domain simulation techniques have been developed to estimate the time domain waveforms in recent years, general multi-conductor cases where frequency dependent characteristics of the transmission lines have a great impact on overall time domain waveform remain one of the most difficult problems. Most recent techniques are based on the approximation of the system functions of the transmission line. The typical approximation techniques are Padé approximations [48], which is the pioneer work in this field, Padé approximation via Lanzos process [49], block Arnoldi [50], Prony's method [45, 51], interpolation approximation using difference model [52], recursive convolution [53], mini-max methods, least square methods, etc. Even though there are shortcomings associated with these techniques such as inaccuracy, instability, inefficiency, and incompatibility with existing simulators, constant improvements have been made. However, the most time consuming part of the simulation is not related to the time domain simulation techniques themselves but to the frequency dependent parameter extractions, which are required for the approximations of the transfer function. A simple approximation using square root dependence of the skin effect can be used to reduce the simulation time [47], yet it still requires two frequency samples (at one high frequency point and one low frequency point) and can be inaccurate when the proximity effect is considerably large. In any cases, these techniques are implemented into a general method of characteristics [54] to obtain time domain waveform at the input and output ports of the multi-conductor transmission lines.

In this chapter, to take advantage of the efficiency of the SRM, SRM will be reformulated in the time domain. Then, two simulation techniques, the general method of characteristics and time domain finite difference method, will be applied

to solve time domain SRM equations. In chapter 2, a minimum segmentation scheme was introduced to reduce the CPU time as well as memory usage in frequency domain SRM. In this chapter, this scheme is used in the time domain simulation technique without lose of accuracy, and from this point, the SRM utilizing the minimum segmentation scheme will be simply noted as the SRM.

4.1 Time Domain Formulation of the SRM

When equation (2.11) is formulated for partial impedance and for transmission line simulation, the return path through the ground conductor has to be considered. In general frequency domain simulation, nodal analysis is often used to include return current effects (2.18). Here, the ground plane itself is divided into several sections, and one arbitrary section is considered as ground, while the rest of the sections are considered to be signals. Then all the transmission line parameters are obtained with respect to this ground section. To satisfy the KVL and the KCL, the voltage of signal sections with respect to this ground section is V_i for sections belong to the signal conductor i , while zero for sections belong to the ground conductor. This technique is well described in [6] for the volume filament technique and is valid as long as the potential is constant across the cross-section of the conductor. After applying this technique, the diagonal matrix $[Z_{ei}]$ in (2.11) becomes

$$Z_{ei,ij}^l = \begin{cases} Z_{ei,ij}^p + Z_{ei,00}^p, & i = j \\ Z_{ei,00}^p, & i \neq j \end{cases}, \quad (4.1)$$

where $Z_{ei,00}^p$ is the EII of the ground ribbon (0th ribbon) and the partial inductance in (2.11) can be converted into a loop inductance using

$$L_{ij}^l = L_{ij}^p + L_{00}^p - L_{i0}^p - L_{0j}^p, \quad (4.2)$$

where L_{00}^p is the partial self inductance of the ground ribbon, L_{ij}^p is the partial inductance between ribbon i and j . These values can be calculated easily using closed form equations [5]. After applying (4.1) and (4.2), (2.11) becomes

$$([Z_{eii}^l] + j\omega[L^l])[I_n] = -\frac{\partial}{\partial z}[V_n], \quad (4.3)$$

where $[V_n]$ and $[I_n]$ are the node voltage vector and node current vector respectively, $[Z_{eii}^l]$ and $[L^l]$ are $(N_f - 1) \times (N_f - 1)$ square matrices that are the loop matrices with respect to the ground section. In (4.3), each element of $[Z_{eii}^l]$ can be easily represented with a polynomial rational function using the equivalent RL circuit model for the EII

$$Z_{eii}^p(s) = R_1 \frac{s^3 + a_2 s^2 + a_1 s + a_0}{s^3 + b_2 s^2 + b_1 s + b_0}. \quad (4.4)$$

Rewriting (2.11) in the s-domain after applying (4.1) and (4.2) results in

$$\frac{1}{s}[Z_{eii}^l(s)]s[I] + s[L^l][I] = -\frac{\partial}{\partial z}[V]. \quad (4.5)$$

Taking the inverse Laplace transform on both sides of (4.5) results in

$$[\xi(t)] * \frac{\partial}{\partial t}[I(t)] + [L^l] \frac{\partial}{\partial t}[I(t)] = -\frac{\partial}{\partial z}[V(t)], \quad (4.6)$$

where $[\xi(t)] = L^{-1}([Z_{eii}^l(s)]/s)$; this matrix can be easily expressed as exponential forms using (4.4). Equation (4.6) has to be solved with

$$[G^l][V(t)] + [C^l] \frac{\partial}{\partial t}[V(t)] = -\frac{\partial}{\partial z}[I(t)]. \quad (4.7)$$

Note that all the elements of $[\xi(t)]$ are in exponential form in (4.6). If one of the functions that is involved in the convolution is in exponential form, approximated recursive relationship can be derived as follows:

$$v(t) * e^{pt} \Big|_{t=(n+1)\Delta t} = \int_0^{n\Delta t} v(\tau) e^{p((n+1)\Delta t - \tau)} d\tau$$

$$\begin{aligned}
&= \int_0^{n\Delta t} v(\tau) e^{p((n+1)\Delta t - \tau)} d\tau + \int_{n\Delta t}^{(n+1)\Delta t} v(\tau) e^{p((n+1)\Delta t - \tau)} d\tau \\
&= e^{p\Delta t} \int_0^{n\Delta t} v(\tau) e^{p(n\Delta t - \tau)} d\tau + \int_{n\Delta t}^{(n+1)\Delta t} v(\tau) e^{p((n+1)\Delta t - \tau)} d\tau \\
&\approx e^{p\Delta t} \int_0^{n\Delta t} v(\tau) e^{p(n\Delta t - \tau)} d\tau + \Delta t v((n+1)\Delta t), \tag{4.8}
\end{aligned}$$

where backward Euler integration is used to approximate the integral. Applying the formulation (4.8) to the first term of left hand side of (4.6) at $t = n\Delta t$ results in

$$\begin{aligned}
&\Delta t [K] \frac{\partial}{\partial t} [I(n\Delta t)] + [e^{-p\Delta t}] \left\{ [\xi((n-1)\Delta t)]^* \frac{\partial}{\partial t} [I((n-1)\Delta t)] \right\}, \\
&+ [L^l] \frac{\partial}{\partial t} [I(n\Delta t)] = - \frac{\partial}{\partial z} [V(n\Delta t)] \tag{4.9}
\end{aligned}$$

where $[K]$ consists of residues of the polynomial rational function, and $Z_{ei,ij}^l(s)/s$, and the p 's are poles of this rational function. The first term of (4.9) can be ignored if Δt is chosen such that the third term is much bigger than this term.

4.2 Method of Characteristics (MC)

In a homogeneous medium (4.7) and (4.9) can be solved easily since the product $[L^l][C^l]$ is a diagonal matrix that has identical eigenvalues. The method of characteristics (MC) was first introduced by Branin [55] for a single lossless line simulation. Later this method was extended to general multi-conductor cases including nonlinear transmission lines with frequency dependency [56]. The MC solves partial differential equations by transforming them into ordinary differential equations along the characteristic directions. This method has been used in conjunction with other transfer function approximation techniques to accelerate time domain simulation [52, 54, 57-59]. In the general method of characteristics (MC), the N coupled transmission lines are treated as a $2N$ port network. The propagation speed of forward and backward waves for the de-coupled modes is

$$v = \frac{dz}{dt} = \pm \frac{1}{\sqrt{\lambda}}, \quad (4.10)$$

where λ is an eigenvalue of $[L'] \cdot [C']$, which is the diagonal matrix $[\mu\epsilon]$ in a homogeneous medium. Applying this relationship to (4.7) and (4.9) gives,

$$d\left(V(n\Delta t) \pm \frac{1}{\sqrt{\lambda}} [L'] I(n\Delta t)\right) / dt = -\left(\frac{1}{\sqrt{\lambda}} E_{ds}((n-1)\Delta t) \pm \frac{1}{\lambda} [L'] [G'] [V]\right), \quad (4.11)$$

where E_{ds} is the voltage source per unit length representing the second term of equation (4.9), which only depends on the values of the previous time step. For a low substrate loss and uniform cross-sectional lines, (4.11) can be expressed using a trapezoidal integral rule as

$$\{V + v[L']I + 0.5\Delta t E_{ds} v\}(z + \Delta z, t + \Delta t) = \{V + v[L']I - 0.5\Delta t E_{ds} v\}(z, t), \quad (4.12)$$

$$\{V - v[L']I - 0.5\Delta t E_{ds} v\}(z - \Delta z, t + \Delta t) = \{V - v[L']I + 0.5\Delta t E_{ds} v\}(z, t), \quad (4.13)$$

where (4.12) and (4.13) are for the forward travelling wave and backward travelling wave, respectively.

Equation (4.12) and (4.13) are the basis of the simulation technique. To solve these two equations, first, the length of each section (i.e. Δz), the distance between two adjacent points where the voltages to be calculated must be determined. For short uniform lines this can be large, which will save considerable CPU time. The procedure of using (4.12) and (4.13) is well described in [56]. In this method, the voltages and currents at the input and output terminals are calculated at each time step, and the implementation of this method into other conventional simulation programs such as SPICE to simulate transmission lines with other non-linear elements is possible. In inhomogeneous medium, several different modes are travelling at different speeds and the application of MC is difficult unless the telegrapher's equations are de-coupled. The various techniques [44, 56, 58, 59] attempt to de-couple the equations through eigenvectors of $[L][C]$ and $[C][L]$. By using these two eigenvector matrices, the inductance and capacitance matrices can be

diagonalized. After the diagonalization, equations similar to (4.12) and (4.13) can be derived and MC can be applied to solve these equations. The numerical details in this matter will be dealt with in a later section. Other techniques that solve problems in the frequency domain directly then transform the results into the time domain have been used successfully, yet the stability and accuracy of these techniques with nonlinear circuits as well as the requirements for good frequency domain samples will be bottlenecks for these techniques. In the next section, the finite difference method (FD) is applied to solve the problems in an inhomogeneous medium.

4.3 Finite Difference Method

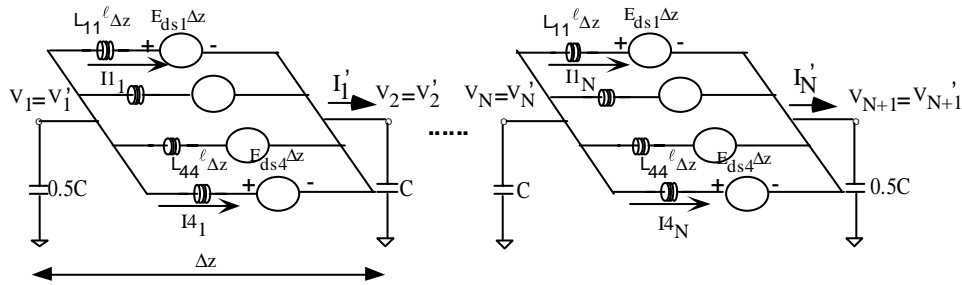


Figure 4.1): An equivalent circuit model for the finite difference method. In each branch, a voltage source is used to replace a ladder model and is responsible for the frequency dependent effects in time domain.

The finite difference method is based on the π equivalent circuit model shown in figure 4.1 that is an equivalent circuit model for (4.7) and (4.9). This method, also referred to as a time-stepping solution, makes a finite difference approximation to (4.7) and (4.9). In the FD method, to achieve a greater stability and accuracy, the electric field nodes and magnetic field nodes are separated by $\Delta z/2$ [13] [60]. This constraint is similar to the FDTD method, which solves Maxwell's equations in 3-dimensional space and time domain using Yee's cell [61]. The

equivalent circuit model in Figure 4.1 shows a total of N lumped sections are used and the voltage nodes, V_1, V_2, \dots, V_{N+1} and current nodes, $I_1^i, I_2^i, \dots, I_N^i$, are separated by $\Delta z/2$. The finite difference approximation of (4.7) and (4.9) at $t = n\Delta t$ and node m gives

$$[I_m((n+1)\Delta t)] = [I_m(n\Delta t)] - \frac{\Delta t}{\Delta z} [L^i]^{-1} \left\{ [V_{m+1}'(n\Delta t)] - [V_m'(n\Delta t)] + \Delta x [E_{ds,m}(n\Delta t)] \right\} \quad (4.14)$$

$$[V_{m+1}((n+1)\Delta t)] = \left\{ \frac{\Delta z}{\Delta t} [C] + \frac{\Delta z}{2} [G] \right\}^{-1} \left(\left\{ \frac{\Delta z}{\Delta t} [C] - \frac{\Delta z}{2} [G] \right\} [V_{m+1}(n\Delta t)] \right. \\ \left. - [I_{m+1}'(n\Delta t)] + [I_m'(n\Delta t)] \right), \quad (4.15)$$

where $[U]$ is the identity matrix, $m = 1, 2, \dots, N$ for (4.14) and $m = 1, 2, \dots, N-1$ for (4.15). Here, the voltage and current vectors indicated with primes on the right hand side of (4.14) and (4.15) can be obtained from original vectors through the KVL and the KCL (figure 4.1). For instance, in (4.14), $[I_m']$ is calculated through the relationship

$$I_m' = I1_m + I2_m + I3_m + I4_m.$$

The boundary conditions for capacitance or resistance termination can be easily applied using the equivalent circuit shown in Figure 4.1. Assuming resistance termination at the input end and capacitance termination at the output end, the boundary condition becomes

$$[V_1((n+1)\Delta t)] = \left\{ [R_s][C] \frac{\Delta z}{\Delta t} + \frac{[R_s][G]\Delta z}{2} + [U] \right\}^{-1} \left(\left\{ [R_s][C] \frac{\Delta z}{\Delta t} - \frac{[R_s][G]\Delta z}{2} - [U] \right\} [V_1(n\Delta t)] \right. \\ \left. - 2[R_s][I_1(n\Delta t)] + [V_s(n\Delta t)] + [V_s((n+1)\Delta t)] \right)$$

(4.16)

$$[V_{N+1}((n+1)\Delta t)] = \left\{ \frac{[C]\Delta z}{2\Delta t} + \frac{[C_L]}{\Delta t} + \frac{[G]\Delta z}{4} \right\}^{-1} \left(\left\{ \frac{[C]\Delta z}{2\Delta t} + \frac{[C_L]}{\Delta t} - \frac{[G]\Delta z}{4} \right\} [V_{N+1}(n\Delta t)] \right. \\ \left. + [I_N(n\Delta t)] + \frac{[C_L]}{\Delta t} [V_L((n+1)\Delta t)] - [V_L(n\Delta t)] \right), \quad (4.17)$$

where $[R_s]$ and $[C_L]$ are source resistance and termination capacitance matrices, and $[V_s]$ and $[V_L]$ are source and termination voltage source vectors. To insure the stability the Courant condition has to be satisfied such that

$$\Delta t \leq \frac{\Delta z}{v}, \quad (4.18)$$

where v is the propagation velocity. However, for multiconductor transmission lines in an inhomogeneous medium, there are several different modes travelling at different speeds. To determine the speed of each mode, eigenvalues of the matrix product $[L][C]$, λ_i , can be used

$$v_i = \frac{1}{\sqrt{\lambda_i}} \quad i = 1, 2, \dots, N_c. \quad (4.19)$$

To ensure the stability the maximum v_i is used to choose Δt , i.e., $\Delta t = \Delta z / \max(v_i)$. One conservative way without going through mode separation is calculating v with dielectric constant 1 everywhere. The value of Δz mainly depends on the rise time of the input signal and the length of the transmission line. Once Δz and Δt are determined, (4.16) is used to satisfy the boundary condition at the input end. Then voltages and currents at each node are determined alternately using (4.15) and (4.14). Finally, the boundary condition (4.17) is used to estimate the waveform at the output end. This procedure is repeated at each time step. Because of this iteration step, it is important to choose steps wisely to reduce the CPU time. One of the advantages of using the finite difference method is that various sources can be inserted in the middle of the line and once the simulation is done, all the voltages and currents at each node are known, including the ground plane, which can be useful for simultaneous switching noise analysis. For an extremely high-speed digital signal travelling along a long transmission line, this method present an arduous task and other approaches utilizing frequency domain approximation should be used. However, for most practical packaging cases, the number of segments along the line can be quite small.

When the ground plane is not wide, or when the low frequency inductance does not affect the time domain simulation, the number of sections used for the ground, N_g , can be 1. However, for accurate time domain simulation, current crowding effects and the skin effect in the ground should be included.

4.4 Wide Ground Plane Consideration

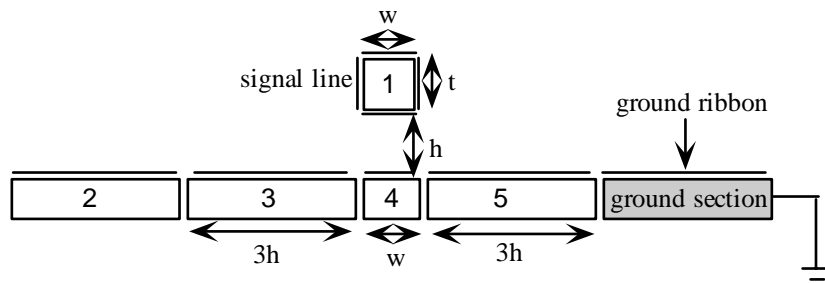


Figure 4.2): Ground plane segmentation and capacitance calculation scheme.

The effect of the finite thickness, conductivity, and the width of the ground plane is often ignored in time domain simulation since the resistance of the wide ground plane is much smaller than that of the signal lines. However, the current crowding effect can change the total inductance value significantly, especially when the signal lines are very close to the ground plane. This change of inductance as a function of frequency can affect the time domain waveform and should be included in the equivalent circuit model. In the SRM, the ground plane is divided into several sections just like signal lines. The number of divisions can be reduced using the minimum segmentation scheme described in [28]. To calculate the series impedance of the ground plane, the plane is divided into N_g sections and each section is represented with a ribbon and the EII approximated with the surface impedance of a plate given in (2.22).

The equivalent circuit of this surface impedance can be obtained using table 3.2 as described in the previous chapter. Then the loop series impedance matrices, $[L]$ and $[Z_{ei}^l]$, are obtained easily by using (4.1) and (4.2). For capacitance matrix calculation, one of the sections on ground plane, the same section that was chosen as a ground for series impedance calculation in (4.1) and (4.2), is considered as ground while other sections are considered as signal conductors. Then the $(N_c + N_g - 1) \times (N_c + N_g - 1)$ capacitance matrix is calculated with respect to the ground section, where N_c is the number of signal conductors. This scheme is illustrated in figure 4.2. After the calculation of the capacitance matrix, (4.14) to (4.17) are used to evaluate the time domain waveform. Here, all the node voltages of the sections belonging to the ground plane are zero, i.e., $V_2, V_3, V_4, V_5 = 0$ in figure 4.2, assuming that the conductor cross sections are equi-potential.

In the finite difference method, the simulation time and memory usage can be significantly reduced without much loss of accuracy by assuming a perfect ground section (but not perfect ground). This will make the matrix $[Z_{ei}^l]$ diagonal and this assumption would be justified if one chose the ground section to be wide such that the resistance of this section is much lower than other sections belonging to the ground plane in figure 4.2. The computation time can be further reduced using a single dominant pole approximation for $[Z_{ei}^l(s)]$.

4.5 Mode De-coupling of the Transmission Line Equation

For the lossless lines in inhomogeneous medium, there are sets of conductor voltages and currents for which the propagation is non-dispersive. These sets, which are called eigenmodes, can de-couple the transmission lines equations where N_c different modes are travelling at any given time. This is based on the fact that both $[L]$ and $[C]$ matrices are positive definite, and the matrix $[L][C]$ can be reduced to diagonal form using the similarity transform

$$[L][C] = [P][\lambda]^2[P]^{-1}, \quad (4.20)$$

where $[P]$ is the eigenvector matrix of $[L][C]$ and $[\lambda]$ is the diagonal eigenvalue matrix of $[L][C]$. Two coupled equations for the transmission lines are

$$\frac{\partial^2[V]}{\partial z^2} = [L][C] \frac{\partial^2[V]}{\partial t^2}, \quad (4.21a)$$

$$\frac{\partial^2[I]}{\partial z^2} = [C][L] \frac{\partial^2[I]}{\partial t^2}, \quad (4.21b)$$

where $[V]$ and $[I]$ are voltage and current vectors respectively. Substituting (4.20) to (4.21a) results in

$$\frac{\partial^2([P]^{-1}[V])}{\partial z^2} = [\lambda]^2 \frac{\partial^2([P]^{-1}[V])}{\partial t^2}. \quad (4.22)$$

Equation (4.22) is the de-coupled equation of (4.21a) and the same procedure can be done for (4.21b) using eigenvector and eigenvalue matrix of $[C][L]$. Now MC can be easily applied to the de-coupled equation (4.22) with characteristic admittance given as

$$[Y_0] = [L]^{-1}[P][\lambda][P]^{-1}. \quad (4.23)$$

A similar method is applied to the lossy lines with series impedance and admittance, $[Z]$ and $[Y]$, replacing the inductance and capacitance, $[L]$ and $[C]$. However, for time domain simulation, frequency dependent components have to be expressed as approximated polynomial rational functions. Obtaining a polynomial rational function for the eigenvector matrix of $[Z][Y]$ is not always easy since approximated poles can reside on the right hand side of the axis, which causes instability. [52], to overcome this problem, the use of the frequency dependent eigenvector matrices is avoided by separating the delay part from the propagation function. Here, delay is estimated using asymptotic value of capacitance and inductance. This approach is implemented on Hspice [47] for multi-conductor analysis. However, as will be

discussed in the next section, this method has numerical problems when the lines are lossy.

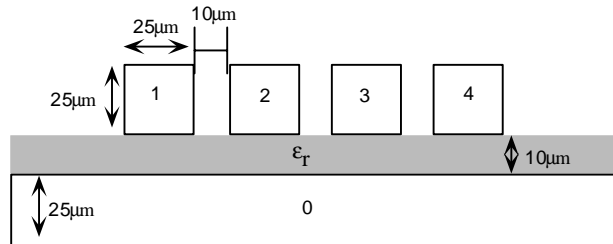


Figure 4.3): Four signal lines above ground plane for skin effect and proximity effect simulation.

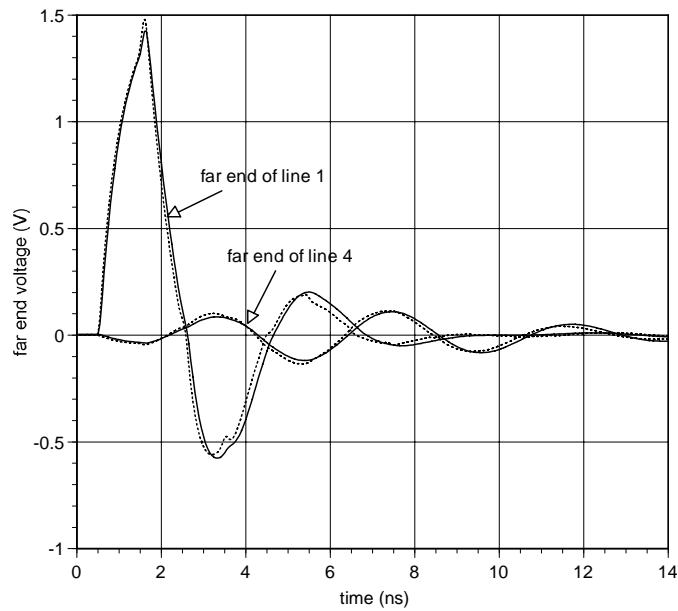
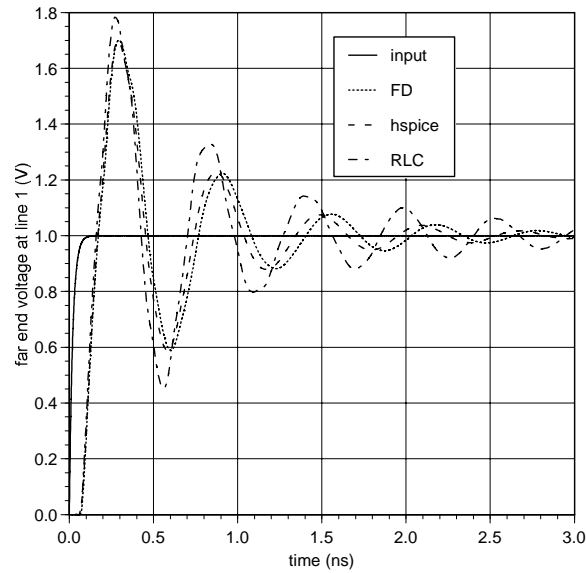
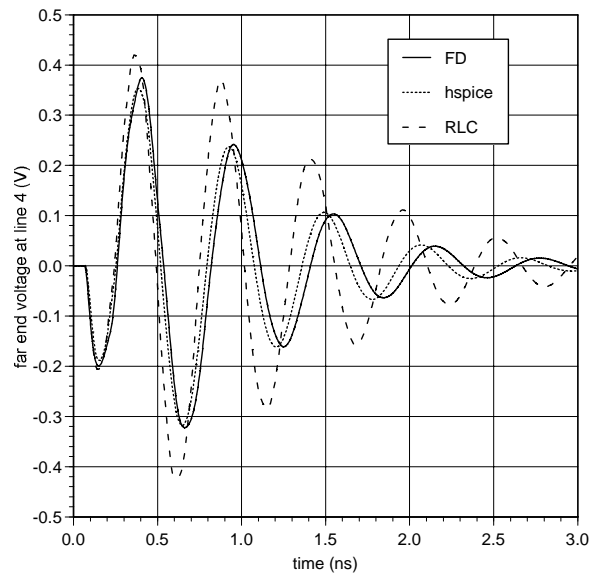


Figure 4.4): Time domain simulation using MC for four line case (Figure 4.3). Solid line: FFT, dotted line: MC.



(a)



(b)

Figure 4.5: Time domain simulation results using various different techniques. FD: finite difference method introduced in this dissertation (Figure 4.1), Hspice: Hspice using W-element, RLC: R-L-C circuit model. (a) Line 1, (b) Line 4.

The separation of the modes can provide valuable information about the transmission line system. For instance, for a system of two symmetric signal lines, there are two distinctive modes: common mode and difference mode. For this particular system, eigenvectors of the matrix $[Z][Y]$ are (1,1) and (1,-1). The common mode has eigenvector (1,1) and its corresponding eigenvalue γ_1^2 , while the difference mode has eigenvector (1,-1) and its corresponding eigenvalue γ_2^2 . If the series impedance and parallel admittance matrices are defined as $[Z]=[R]+j\omega[L]$ and $[Y]=[G]+j\omega[C]$, respectively, the complex modal propagation constants $\gamma_n = \alpha_n + j\omega\beta_n$ ($n=1,2,\dots,N$) and the voltage eigenvector matrix $[P]$ are solutions of the eigenvalue equation [44]

$$(\gamma^2[I]+[Z][Y])[P]=0. \quad (4.24)$$

Depending on the polarity and the magnitude of the signal applied to each line, one mode may dominate the other. Therefore, by inspecting the characteristics of each mode, one may predict the behavior of the multiple lines. For instance, if the polarity of a pair of voltages applied to two signal lines is (1,1), then common mode becomes a dominant mode. Typical on-chip interconnect structures consist of multiple pairs of orthogonal metal layers as shown in Figure 4.6 (see Table 4.1 for dimensions used in the simulation). To accurately simulate the time domain response, the impact of the orthogonal lines has to be considered. Figure 4.7 shows the attenuation constant and the propagation time constant of metal lines on layer 5 when there are no orthogonal lines (Figure 4.7a, 0% loading) and when there are orthogonal lines (Figure 4.7b, 100% loading). When there are no orthogonal lines, the difference mode is clearly attenuated more and has slower propagation time than the common mode for most of the frequency range interested. Once the orthogonal line impact is included in the simulation, common mode becomes slower than the

difference mode (see Figure 4.7b). Also the difference of the attenuation constants between two modes becomes smaller. This is because the orthogonal lines significantly increase the self-capacitance and the common mode is more affected by the change of the self-capacitance.

	Layer 3 (in μm)	Layer 4 (in μm)	Layer 5 (in μm)	Layer 6 (in μm)	Layer 7 (in μm)	Layer 8 (in μm)
t_i (thickness)	0.3	0.3	1	1	2	2
W (width/space)	0.13	0.13	1	1	2	2
h_i	0.3	0.3	1	1	2	-

Table 4.1. Dimensions of the metals on each layer (lines are assumed to be copper, the space between the lines is the same as the width of the line).

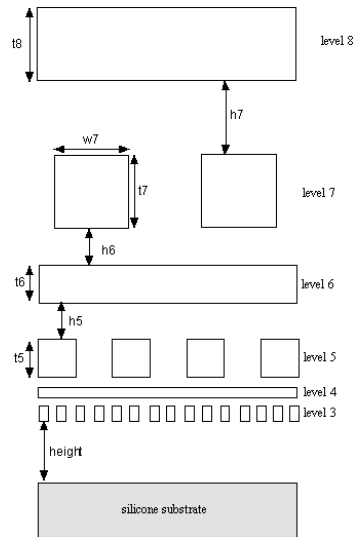


Figure 4.6) Typical on-chip interconnect structure.

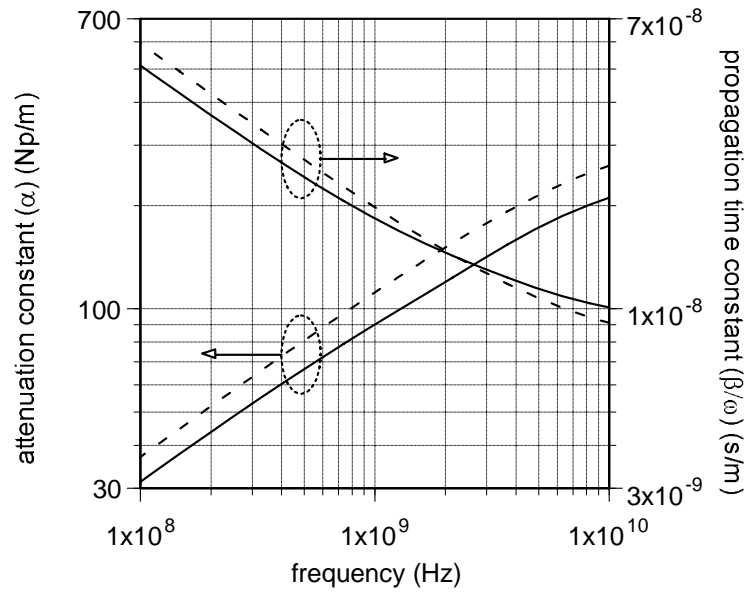


Figure 4.7 (a) Frequency dependent attenuation constant and propagation time constant when there are no adjacent orthogonal lines. Solid line: common mode, Dashed line: difference mode.

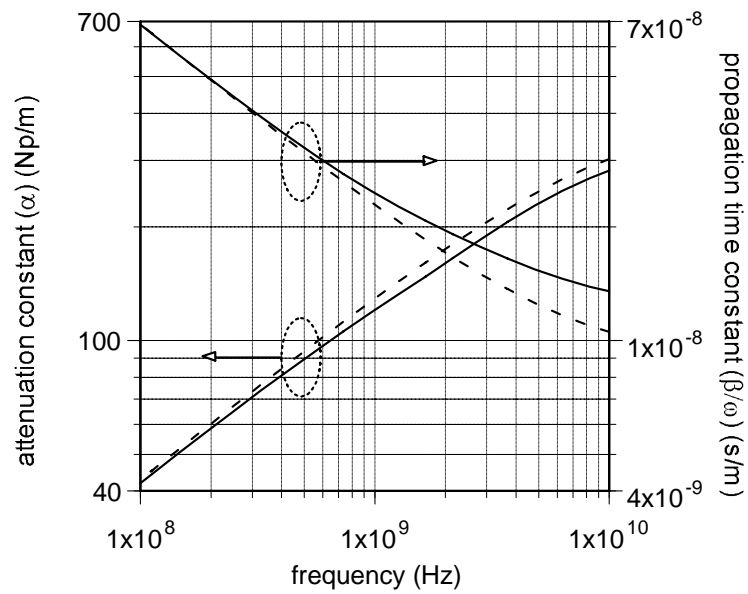


Figure 4.7 (b) Frequency dependent attenuation constant and propagation time constant when there are adjacent orthogonal lines (100% loading). Solid line: common mode, Dashed line: difference mode.

To illustrate this point, time domain simulation is performed. Two symmetrical lines without adjacent orthogonal lines are excited with two positive rising signals with 10ps rise time. Then the result is compared with the case when two lines are excited with two opposite polarity voltages with rise/fall time 10ps (Figure 4.8a). The same simulation is carried out with the presence of the orthogonal lines (Figure 4.8b). It is clear that the common mode is faster and less degraded than the difference mode in the absence of the orthogonal lines, as seen in Figure 4.8a. On the other hand, Figure 4.8b shows that the faster difference mode arrives at the far end first.

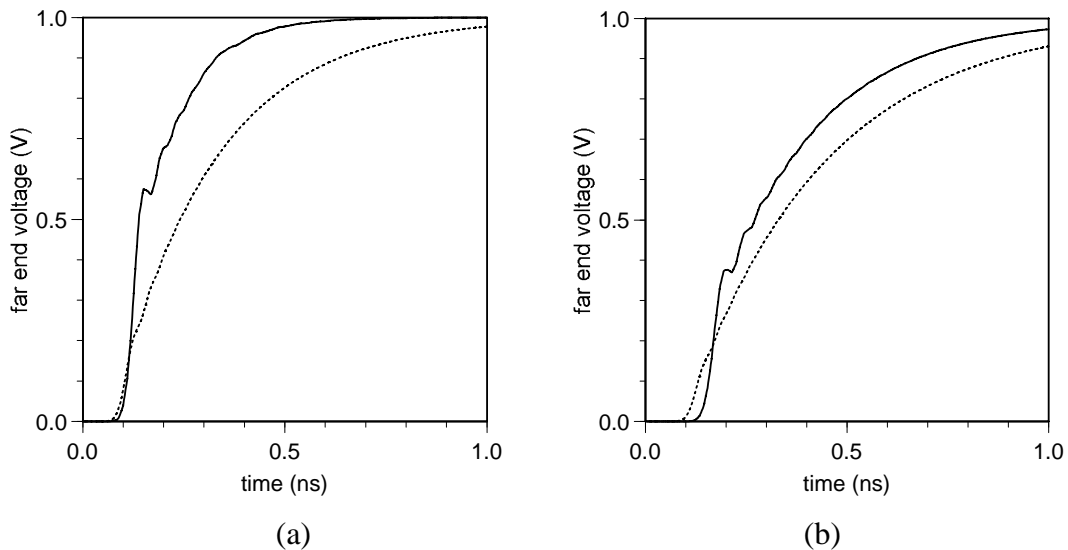


Figure 4.8) Far end time domain simulation of two symmetrical lines on metal layer 5 shown in Figure 4.6. Line length=10mm, source resistance=30ohms, open termination. (a) When there are no adjacent orthogonal lines, (b) when there are orthogonal lines (100% loading). Solid line: voltage applied with the same polarity, dotted line: voltage applied with the opposite polarity.

However, due to the higher attenuation constant, the difference mode is more degraded than the common mode resulting in longer time delay at the 50% point (0.5V). This result suggests that the attenuation constant is the more determining factor in estimating the delay for this particular case. The dimension of the conductors in this simulation is small and the resistance dominates the reactance.

4.6 Results and Discussions

As a first example, the case of four lines above the ground plane in a homogeneous medium is tested with MC. All the ground effects are included in the equivalent circuit. The dimensions of the signal lines are 20 μm wide, 20 μm thick, 0.1m long, separated by 10 μm . The ground plane is 170 μm wide, 20 μm thick, and the distance between ground and signal conductors is 10 μm . All the lines are copper and terminated with 10pF capacitance and the source resistance is chosen to be 5 Ω . The medium surrounding these lines is assumed to be air. This example is shown in figure 4.3 and it is set up such that all the skin effect and proximity effects as well as ground plane current crowding effects contribute to the time domain simulation results. The trapezoidal input wave is applied to line 1 with rise and fall time 0.1ns and duration of 1ns. The results are compared with the FFT method. Figure 4.4 shows great agreement between FFT and MC. The CPU time for this case on 266MHz Pentium II is 7.6 second.

In the next example, all the dimensions of the signal conductors are the same as the previous example except the ground plane width is changed to be 500 μm , the length of the lines are assumed to be 2cm, and the dielectric constant between signal lines and ground plane is assumed to be 4. This time, line 1, 2, and 3 are switching with an exponential wave

$$V_{in} = 1 - e^{-5 \cdot 10^{10} t} . \quad (4.25)$$

Figure 4.5 shows the results and comparison with Hspice® W-Element that uses frequency domain transfer function approximation method simulated with MC. The slight difference between the Hspice result and the finite difference method is due to the lack of the frequency dependent inductance in Hspice. Also shown is the simulation results of constant RLC model that ignores skin effect. Here, DC resistance and high frequency L and C are used. Figure 4.5 clearly shows ignoring frequency dependent series resistance can cause erroneous results. The computation time for FD method is 5 seconds.

It has been observed that some frequency domain approximation methods can generate an unstable waveform that is not possible under normal conditions. The third example is for 125mm long copper line with 2.5 μ m width, 2.5 μ m thickness and 2.5 μ m above a 13 μ m wide ground plane. The source resistance is 80ohms, the termination capacitance is 0.1pF, and a 10ns rise time input wave is applied. Under these conditions, skin effect is not a major factor for time domain simulation and constant RLC circuit or even RC circuit model should be enough to get reasonable results. The current passing source resistance is simulated with FD method described in this dissertation, constant RLC model and Hspice. As figure 4.9 indicates, unlike the Hspice result, the FD method and RLC circuit model do not show continuous negative current that can cause constant overshoot voltage, which is not possible for a stable system. When a line is extremely lossy, as in this particular example, the delay time is dominated by the RC delays and does not depend on the inductance of the line. The technique used in Hspice W-element that separates LC delay from the propagation function to avoid instability can actually cause instability in RC line analysis.

In chapter 3, the conditions where frequency dependent series impedance has to be included in the circuit model to get an accurate time domain response were discussed. To verify these conditions, the same four line structure shown in figure 4.3 is used (5 ohms source resistance, 10pF termination, 0.1ns rise and fall time input

with 1ns duration). The result from the FFT method is compared with the results obtained under the following assumptions:

- 1) Lines are modeled with LC lines.
- 2) Lines are RLC lines (R_{dc} - L_{ext}).
- 3) Lines are $R(f)$ LC lines (Hspice W-element).

Figure 4.10 shows that failing to include all the frequency dependent effects in the model result in erroneous time domain waveforms.

In this chapter, new RLC equivalent circuit model including frequency dependent series impedance were introduced. To reduce computation time, the method of characteristics and finite difference method are used. Since this technique easily generates an equivalent circuit from the geometry of the conductors and simple closed form equations, it avoids extraction of the frequency dependent samples for the approximation of the transfer function in frequency domain. The mode separation is often useful to estimate delays for different switching conditions. The worst case delay estimation can be obtained by simulating only one mode.

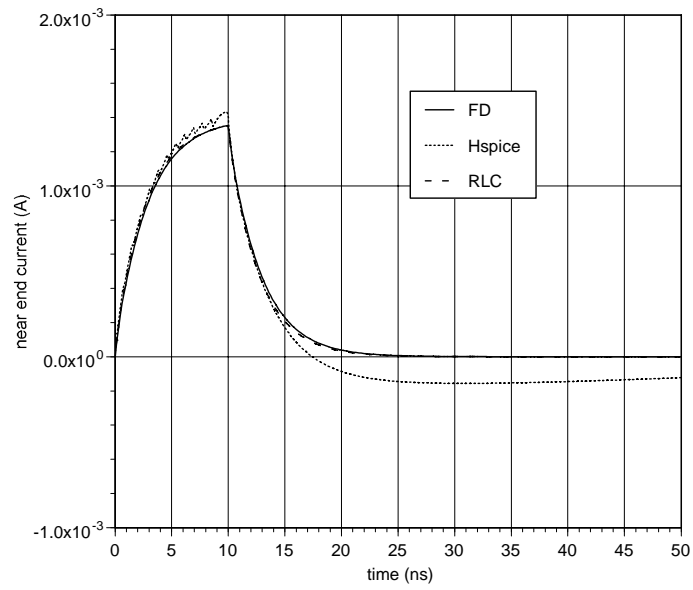
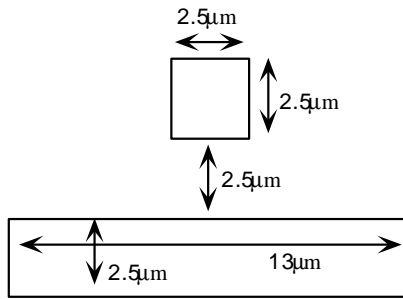


Figure 4.9): Current waveforms at the input terminal.

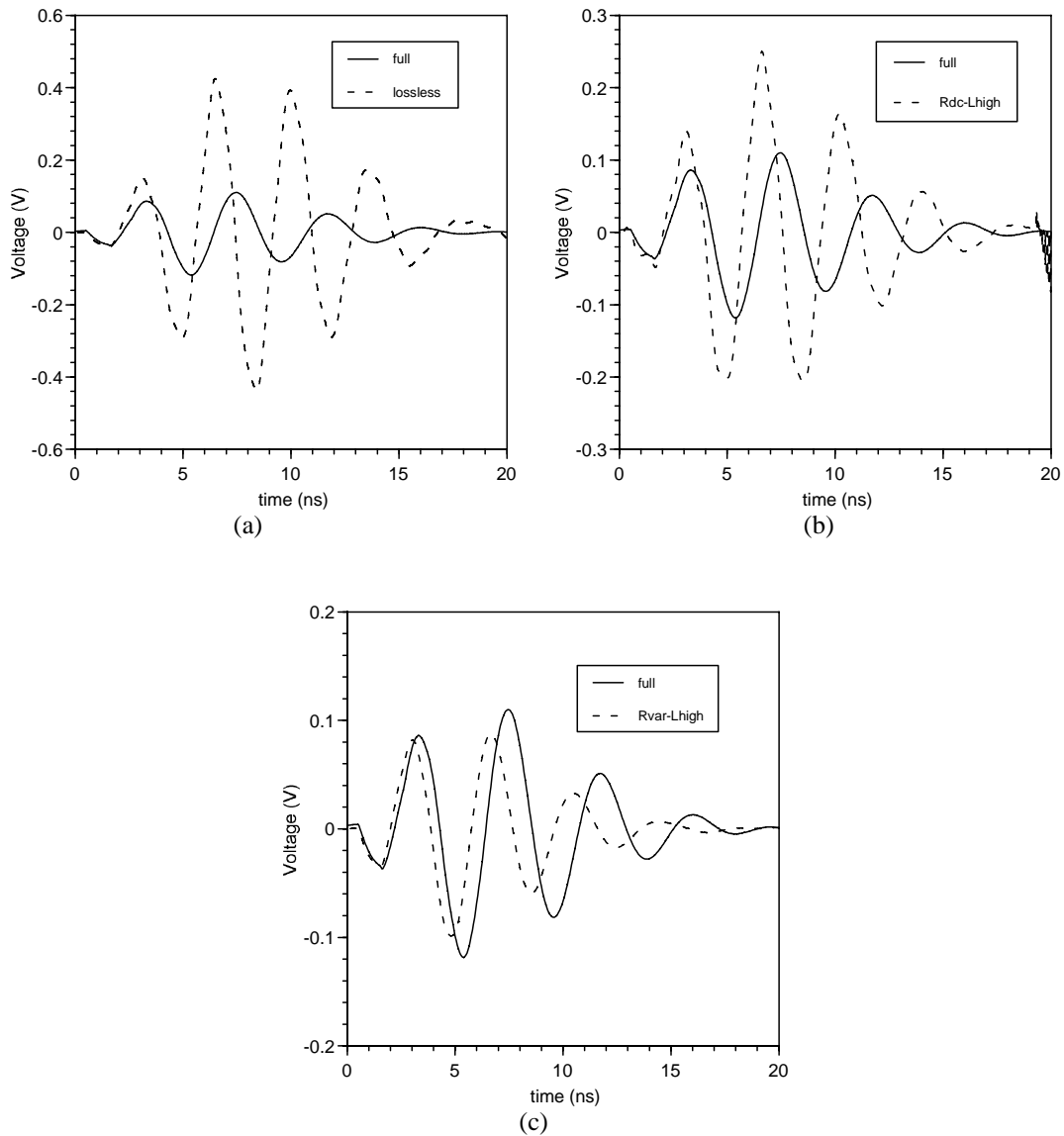


Figure 4.10) Impact of frequency dependent characteristics of the transmission lines on crosstalk (line 4). (a) Comparison between full dispersion curve obtained from FD method and lossless line. (b) Comparison between full dispersion curve obtained from FD method and RLC line (ignoring frequency dependent R and L). (c) Comparison between full dispersion curve obtained from FD method and R(f)LC line (ignoring frequency dependent L).

Chapter 5

Discussions and Conclusions

A new impedance boundary condition (EII) that is useful for series impedance calculation of multi-conductor transmission lines has been introduced. Because of its localized characteristics the EII can be approximated using analytic expressions. Also, by using a transmission line model, approximating the EII of conductors with arbitrary cross-section is possible. The use of the impedance boundary conditions (IBC) has been limited to the scattering problems since most of the IBC are only predictable at high frequency range. Due to the characteristics of the EII, EII can be used in conjunction with other field solvers like FDTD, PEEC, or conformal mapping. In this dissertation, the EII is used with surface integral equations. Since the EII can be approximated using analytical expression, arduous task of finding surface current distribution can be avoided. This new method is called surface ribbon method [11, 12, 28]. Comparing to the volume filament method (VFM), which assumes a constant volume current flowing through filaments, surface ribbon method (SRM) uses equivalent surface current. Further study shows that the number of the surface ribbons along the rectangular surface can be as small as four. Also, wide ground planes that can effect the frequency dependent inductance values can be efficiently included in the analysis. This method also has been extended to three-dimensional structures [10]. However, when the discontinuity portion of the structure is the small part of the overall structure, simple $2\frac{1}{2}$ dimensional approach can be used without sacrificing much accuracy. In chapter 2, the theoretical bases for the EII and the SRM are introduced. Also, the SRM has been applied to arbitrary

cross-sectional conductors. The maximum local error has been estimated compare to the more rigorous volume filament technique.

In chapter 3, SPICE equivalent circuit modeling for both on-chip and off-chip interconnects is explored. RLC circuit models have been widely used due to their ease of integration with other non-linear elements of a circuit in time domain simulation. Most on-chip interconnects are modeled using RC lumped circuits. Simple delay equations based on constant voltage source driving an RC line might overestimate the delays simulated using actual device due to the unique characteristics of the CMOS driver. For accurate estimation of the delay, simulation has to be carried out using RC lumped circuit. Alternative approach is using analytic equation based on the curve fitting the actual simulation result. However, this method has to be carried out for each different generations (different gate length) since the characteristics of the device is different for each generation. In estimating clock cycle time for microprocessor requires thorough estimation of delays. This includes delay due to the device, delay due to the interconnect, and delay due to the clock skew. The delay due to the device will decrease due to the decrease of the device capacitance. The delay due to the interconnect is the most controversial factor among timing analyzers. Some reports speculate the percentage of the interconnect delay will be well over 50% of the total delays. However, this will unlikely happen near future if the low dielectric material and copper metals are used. The global wires that connect separate functional blocks can contribute clock cycle time due to their long length. These lines are driven by the large drivers that have small internal resistance. Also, these lines are fabricated to be “fat” to reduce the RC delays. Accordingly, the inductance has to be included in the circuit model to accurately estimate the delays. Some designers suggest to make the drivers as large as possible to reduce the delays. However, this will not only consume extra area and energy but also can increase the delays or other signal integrity problems. If the driver is much larger than internal circuits, the extra delay is added since the small

internal driver has to drive large external driver. More accurate equivalent circuit modeling including inductance effects becomes essential to predict the overall circuit behavior.

The inductance effects are important when the line resistance and source resistance are comparable to the characteristic impedance of the line. Skin effect and proximity effect have rarely impact on on-chip interconnect. In package level, as signal rise time decreases, these effects have to be considered for accurate time domain analysis. In this dissertation, compact equivalent circuit model that can be simulated with typical simulators like SPICE is introduced. If series impedance at two frequency points is known, simple circuit model consists of 8 resistors and inductors can capture frequency dependency of the transmission line from DC to high skin effect frequency. In this dissertation, an equivalent circuit model based on the SRM is introduced. By using transmission line model of the EII and its equivalent circuit, multiple conductors with arbitrary cross-section can be efficiently modeled. The circuit simulators based on moment matching technique [48] can accelerate the simulation time of this kind of RLC circuit tremendously. Unfortunately the earlier technique based on Padé approximation cannot accurately simulate this type of RL loop circuits even with high order approximation (large number of moments). However, more accurate techniques have been developed, which can be applied to general circuits [49]. These new techniques will allow faster simulation of the RLC circuits introduced in this dissertation.

In chapter 4, the time domain formulation for the SRM is obtained using the equivalent circuit model of EII. This equivalent circuit model can be easily transformed into time domain using polynomial rational function that has three poles and zeros (4 resistors and 3 inductors). The convolution equation that appeared in the time domain SRM equation is solved using recursive equation. Both the method of characteristics (MC) and the finite difference (FD) method are applied to solve time domain SRM equations. Because all the parameters needed for the simulation

are calculated using analytical equations, great numerical efficiency can be achieved. MC is a very efficient time domain transmission line analysis technique. To apply this technique to the general transmission line problems that might be embedded in inhomogeneous medium, mode separation has to be done. For further improvement, the transfer function of the equivalent circuit has to be obtained [53]. The finite difference method is much more flexible since both current and voltage values of each node at each time step are known. However, when a long transmission line is analyzed and the number of time steps is large this method could be inefficient. The most efficient method uses transfer functions of the lines. Frequency samples required for these techniques can be efficiently obtained through the SRM introduced in this dissertation.

Appendix

Inductance Calculation Using Closed Form Equation

The self inductance of a ribbon and mutual inductance between ribbons can be easily calculated using geometric mean distance [62].

1. Self inductance:

According to the geometric mean distance (G.M.D) theorem, G.M.D. of a ribbon with width W is approximated as,

$$G.M.D. = 0.22313W . \quad (1)$$

Applying this to the empirical formula results,

$$\frac{L}{\ell} \approx \frac{\mu}{2\pi} \left[\ln \left(\frac{2\ell}{0.22313W} \right) - 1 \right] \quad (2)$$

where ℓ is the length of the ribbon.

2. Mutual inductance:

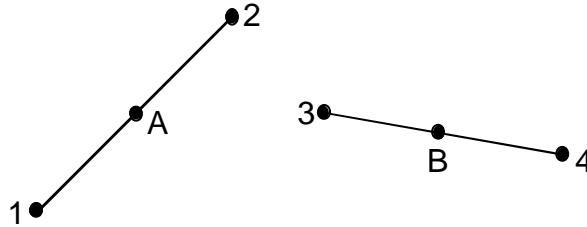


Figure A): two arbitrary oriented ribbons. Length (ℓ) is in perpendicular direction to the paper.

For mutual inductance calculation of two arbitrary oriented ribbons, Rayleigh quadrature formula [62] can be used. From figure A, the approximated mutual inductance is

$$M = \frac{1}{6} (M_{B1} + M_{B2} + M_{A3} + M_{A4} + 2M_{AB}), \quad (3)$$

where A and B are the midpoints of two ribbons and M_{B1} is the mutual inductance between line filament 1 and B. The mutual inductance between two parallel line filaments can be calculated using

$$\frac{M}{\ell} = \frac{\mu}{2\pi} \left[\ln \left(\frac{\ell}{d} + \sqrt{1 + \frac{\ell^2}{d^2}} \right) - \sqrt{1 + \frac{d^2}{\ell^2}} + \frac{d}{\ell} \right], \quad (4)$$

where d is the distance between two lines.

Two dimensional equations can be obtained assuming $\ell=1\text{m}$.

Bibliography

- [1] "The National Technology Roadmap for Semiconductors," . 1997, Semiconductor Industry Associations.
- [2] C.S. Chang, S. Kim, and P. Fisher, "Design and Technology Considerations for the Future Generations," *IEEE/ACM Tau* 99, 1999.
- [3] D. Sylvester and K. Keutzer, "Getting to the Bottom of Deep Submicron," *IEEE/ACM ICCAD* 98, 1998.
- [4] A. Deutsch, "When are Transmission-Line Effects Important for On-Chip Interconnections?," *IEEE Transactions on Microwave Theory and Techniques*, vol. 45, October 1997, pp.1836-1844.
- [5] A.E. Ruehli, "Inductance Calculations in a Complex Integrated Circuit Environment," *IBM Journal of Research and Development*, Sept. 1972, pp.470-481.
- [6] W.T. Weeks, *et al.*, "Resistive and inductive skin effect in rectangular conductors," *IBM J. Res. and development*, vol. 23 ,1979, pp.652-660.
- [7] M. Kamon, M.J. Tsuk, and J.K. White, "FASTHENRY: A Multipole-Accelerated 3-D Inductance Extraction Program," *IEEE Transactions on Microwave Theory And Techniques*, vol. 42, September 1994, pp.1750-1758.
- [8] M.J. Tsuk and J.A. Kong, "A Hybrid Method for the Calculation of the Resistance and Inductance of transmission Lines with Arbitrary Cross Sections," *IEEE Transactions on Microwave Theory and Techniques*, vol. 39, August 1991, pp.1338-1347.
- [9] R.-B. Wu and J.-C. Yang, "Boundary Integral Equation Formulation of Skin Effect Problems In Multiconductor Transmission Lines," *IEEE Transactions on Magnetics*, vol. 25, July 1989, pp.3013-3015.

- [10] B.-T. Lee, "*Efficient Series Impedance Extraction Using Effective Internal Impedance*," *Electrical and Computer Engineering*. 1996, The University of Texas at Austin.
- [11] E. Tuncer, B.-T. Lee, and D.P. Neikirk, "*Interconnect Series Impedance Determination Using a Surface Ribbon Method*," *IEEE 3rd Topical Meeting on EPEP*, 1994, Monterey, CA.
- [12] S. Kim, *et al.*, "*Effective Internal Impedance Method for Series Impedance Calculations of Lossy Transmission Lines: Comparison to Standard Impedance Boundary Condition*," *IEEE Transactions on Microwave Theory and Techniques*, Submitted 1999.
- [13] T. Itoh and B. Houshmand, "*Time-Domain Methods for Microwave Structures*," *IEEE Press*.
- [14] A.E. Ruehli, "*Equivalent circuit models for three-dimensional multiconductor systems*," *IEEE Transactions on Microwave Theory and Technology*, vol. 22, March 1974, pp.216-221.
- [15] H. Heeb and A.E. Ruehli, "*Three-Dimensional Interconnect Analysis Using Partial Element Equivalent Circuits*," *IEEE Transactions on Circuits and Systems-I*, vol. 39, November 1992, pp.974-982.
- [16] S. Kim and D.P. Neikirk, "*Compact Equivalent Circuit Modeling for the Skin Effect*," *IEEE MTT-s*, 1996, San Francisco, CA.
- [17] C.-S. Yen, Z. Fazarinc, and R.L. Wheeler, "*Time-Domain Skin-Effect Model for Transient Analysis of Lossy Transmission Lines*," *Proceeding of the IEEE*, vol. 70, 1982, pp.750-757.
- [18] T.V. Dinh, B. Cabon, and J. Chilo, "*SPICE Simulation of Lossy and Coupled Interconnection Lines*," *IEEE Transactions on Components, Packaging and Manufacturing Technology-B*, vol. 17, May 1994, pp.134-146.

- [19] E. Tuncer and D.P. Neikirk, "*Efficient Calculation of Surface Impedance for Rectangular Conductor*," *Electronic Letters*, vol. 29, 1992, pp.2127-2128.
- [20] A.R. Djordjevic, T.K. Sarkar, and S.M. Rao, "*Analysis of Finite Conductivity Cylindrical Conductors Excited by Axially-Independent TM Electromagnetic Field*," *IEEE Transactions on Microwave Theory and Techniques*, vol. 33, October 1985, pp.960-966.
- [21] S. Ramo, J.R. Whinnery, and T.V. Duzer, *Fields and Waves in Communication Electronics*. 2nd ed. 1984, New York: Wiley.
- [22] E.M. Deely, "*Surface Impedance Near Edges and Corners in Three-dimensional media*," *IEEE Transactions on Magnetics*, vol. 26, March 1990, pp.712-714.
- [23] E.M. Deely, "*Improved impedance boundary condition for finite elements by cross-coupling at corners*," *IEEE Transactions on Magnetics*, vol. 30, 1994, pp.2881-2884.
- [24] E.M. Deely, "*Avoiding surface impedance modification in BE methods by singularity-free representations*," *IEEE Transactions on Magnetics*, vol. 28, September 1992, pp.2814-2816.
- [25] W. Jingguo, J.D. Lavers, and Z. Peibai, "*Modified Surface Impedance Boundary Condition Applied to Eddy Current Problems*," *IEEE Transactions on Magnetics*, vol. 28, March 1992, pp.1197-1200.
- [26] W. Jingguo and J.D. Lavers, "*Modified Surface Impedance Boundary Condition for 3D Eddy Current Problems*," *IEEE Transactions on Magnetics*, vol. 29, March 1993, pp.1826-1829.
- [27] C.A. Balanis, *Advanced Engineering Electromagnetics*. 1989: JOHN WILEY & SONS.
- [28] B.-T. Lee and D.P. Neikirk, "*Minimum Segmentation in the Surface Ribbon Method for Series Impedance Calculations of Microstrip Lines*,"

IEEE 5th Topical Meeting on Electrical Performance of Electronic Packaging. 1996. Napa, CA.

[29] B. Krauter and L. Pileggi, "Generating sparse partial inductance matrices with guaranteed stability," *International Conference on Computer Aided Design*. 1995.

[30] G.H. Golub and C.F.V. Loan, *Matrix Computations*. 1989, Baltimore: Johns Hopkins University Press.

[31] S. Kim, *et al.*, "*SIMIAN USER'S GUIDE*," 1997, The University of Texas at Austin.

[32] E.F. Miersch and A.E. Ruehli, "Analysis of Lossy Coupled Transmission Lines," *IBM Technical Disclosure Bulletin*, vol. 19, November 1976, pp.2363-2365.

[33] H.A. Wheeler, "Formulas for the skin-effect," *Proceedings of the IRE*, vol. 30 September, 1942, pp.412-424.

[34] L.t. Pillage, R.A. Rohrer, and C. Visweswariah, *Electronic Circuit and System Simulation Methods*: McGraw-Hill.

[35] N.H.E. Weste and K. Eshraghian, *Principles of CMOS VLSI Design*: Addison-Wesley.

[36] R. Otten, "Global Wires Harmful," *International Symposium on Physical Design*. 1998. Monterey, CA.

[37] P.D. Fisher and R. Nesbitt, "The Test of Time," *IEEE circuits and Devices*, vol. March, 1998, pp.37-44.

[38] C.S. Chang, *Electrical Design Methodologies*. Vol. 1. 1989, Materials Park, OH: ASM International.

[39] J. Jin, *The Finite Element Method in Electromagnetics*. 1993: John Wiley & Sons, Inc.

[40] R.K. Gordon and S.H. Fook, "A Finite Difference Approach that Employs an Asymptotic Boundary Condition on a Rectangular Outer Boundary for

Modeling Two-Dimensional Transmission Line Structures," IEEE Transactions on Microwave Theory and Techniques, vol. 41, August 1993, pp.1280-1286.

[41] A.H. Zemanian, "A *Finite-Difference Procedure for the Exterior Problem Inherent in Capacitance Computations for VLSI Interconnections,*" IEEE Transactions on Electron Devices, vol. 35, July 1988, pp.985-992.

[42] J. Venkataraman, *et al.*, "Analysis of Arbitrarily Oriented Microstrip Transmission Lines in Arbitrary Shaped Dielectric Media over a Finite Ground Plane," IEEE Transactions on Microwave Theory and Techniques, vol. 33, October 1985, pp.952-959.

[43] K. Nabors, S. Kim, and J. White, "Fast Capacitance Extraction of General Three-Dimensional Structures," IEEE Transactions on Microwave Theory and Techniques, vol. 40, July 1992, pp.1496-1506.

[44] H. You and M. Soma, "Analysis and Simulation of Multiconductor Transmission Lines for High-Speed Interconnect and Package Design," IEEE Transactions on Components, Hybrids, and Manufacturing Technology, vol. 13, December 1990, pp.839-846.

[45] J.G. Maloney and G.S. Smith, "The use of surface impedance concepts in the finite-difference time-domain method," IEEE Transactions on Antennas and Propagation, vol. 40, January 1992, pp.39-48.

[46] K.S. Oh and J.E. Schutt-Aine, "An Efficient Implementation of Surface Impedance Boundary Conditions for the Finite-Difference Time-Domain Method," IEEE Transactions on Antennas and Propagation, vol. 43, July 1995, pp.660-666.

[47] Meta Software, "Hspice User's Manual,"1996, Avanti corp.

[48] L.T. Pillage and R.A. Rohrer, "Asymptotic Waveform Evaluation for Timing Analysis," IEEE Transactions on Computer Aided Design, vol. 4, April 1990, pp.352-366.

- [49] P. Feldmann and R.W. Freund, "*Efficient linear circuit analysis by Pade approximation via the Lanzos process*," *Proceedings of the Euro-DAC*. 1994.
- [50] M. Kamon, *et al.*, "*Automatic Generation of Accurate Circuit Models of 3-D Interconnect*," *IEEE Transactions on Components, Packaging, and Manufacturing Technology-Part B*, vol. 21, August 1998, pp.225-240.
- [51] J. S. L. Marple, *Digital Spectral Analysis*. 1987, Englewood Cliffs, NJ: Prentice-Hall.
- [52] D.B. Kuznetsov, "*Indirect Numerical Integration, Difference Approximation, and Circuit Simulation of Transmission Lines*," *Electrical Engineering*. 1996, University of Illinois at Urbana-Champaign: Urbana-Champaign, IL.
- [53] S. Lin and E.S. Kuh, "*Transient Simulation of Lossy Interconnects Based on the Recursive Convolution Formulation*," *IEEE Transactions on Circuits and Systems-I: Fundamental Theory and Applications*, vol. 39, November 1992, pp.879-892.
- [54] F.Y. Chang, "*The generalized method of characteristics for waveform relaxation analysis of lossy coupled transmission lines*," *IEEE Transactions on Microwave Theory and Techniques*, vol. 37, December 1989, pp.2028-2038.
- [55] J. F. H. Branin, "*Transient Analysis of Lossless Transmission Lines*," *Proceedings of IEEE*, vol. 55, 1967, pp.2012-2013.
- [56] J.-F. Mao and Z.-F. Li, "*Analysis of the Time Response of Multiconductor Transmission Lines with Frequency-Dependent Losses by the Method of Convolution Characteristics*," *IEEE Transactions on Microwave Theory and Techniques*, vol. 40, April 1992, pp.637-644.
- [57] J.E. Bracken, V. Raghaven, and R.A. Rohrer, "*Interconnect Simulation with Asymptotic Waveform Evaluation (AWE)*," *IEEE Transactions on Circuits and Systems-I*, vol. 39, November 1992, pp.869-878.

- [58] N. Orhanovic, V.K. Tripathi, and P. Wang, "*Time Domain Simulation of Uniform and Nonuniform Multiconductor Lossy Lines By The Method of Characteristics*," *IEEE-s*, 1990, Dallas.
- [59] F. Romeo and M. Santomauro, "*Time-Domain Simulation of n Coupled Transmission Lines*," *IEEE Transactions on Microwave Theory and Techniques*, vol. 35, 1987, pp.131-136.
- [60] S. Kim and D.P. Neikirk, "*Time Domain Multiconductor Transmission Line Analysis Using Effective Internal Impedance*," *IEEE 6th Topical Meeting on Electrical Performance of Electronic Packaging*, 1997, San Jose, CA.
- [61] K.S. Yee, "*Numerical solution of initial boundary value problems involving Maxwell's equations in isotropic media*," *IEEE Transactions on Antennas and Propagations*, vol. 14, May 1966, pp.302-307.
- [62] F. Grover, *Inductance calculations, working formulas and tables*. 1946, New York.

Vita

Sangwoo Kim was born in Seoul, Korea on January 12, 1970, the son of Young-Ja Lee and Hyung-Ju Kim. He entered Hong-Ik University, Seoul, Korea, in 1988. He transferred to Michigan State University, East Lansing, Michigan, in 1990. He received the degree of Bachelor of Science from Michigan State University in May 1993. He entered the Graduate School of The University of Texas at Austin, Austin, Texas, in 1993. During the following years he worked as a research assistant under Professor Dean Neikirk. He received the degree of Master of Science in Engineering in May 1996. During 1998 and 1999, he was employed as a technical intern at SEMATECH.

Permanent Address: 172-82 Yonhee-dong Sudaemoon-ku
Seoul, Korea 120-112

This dissertation was typed by the author.